iScience

CellPress
OPEN ACCESS

Article

Hypoxia-induced HMGB1 promotes glioma stem cells self-renewal and tumorigenicity via RAGE

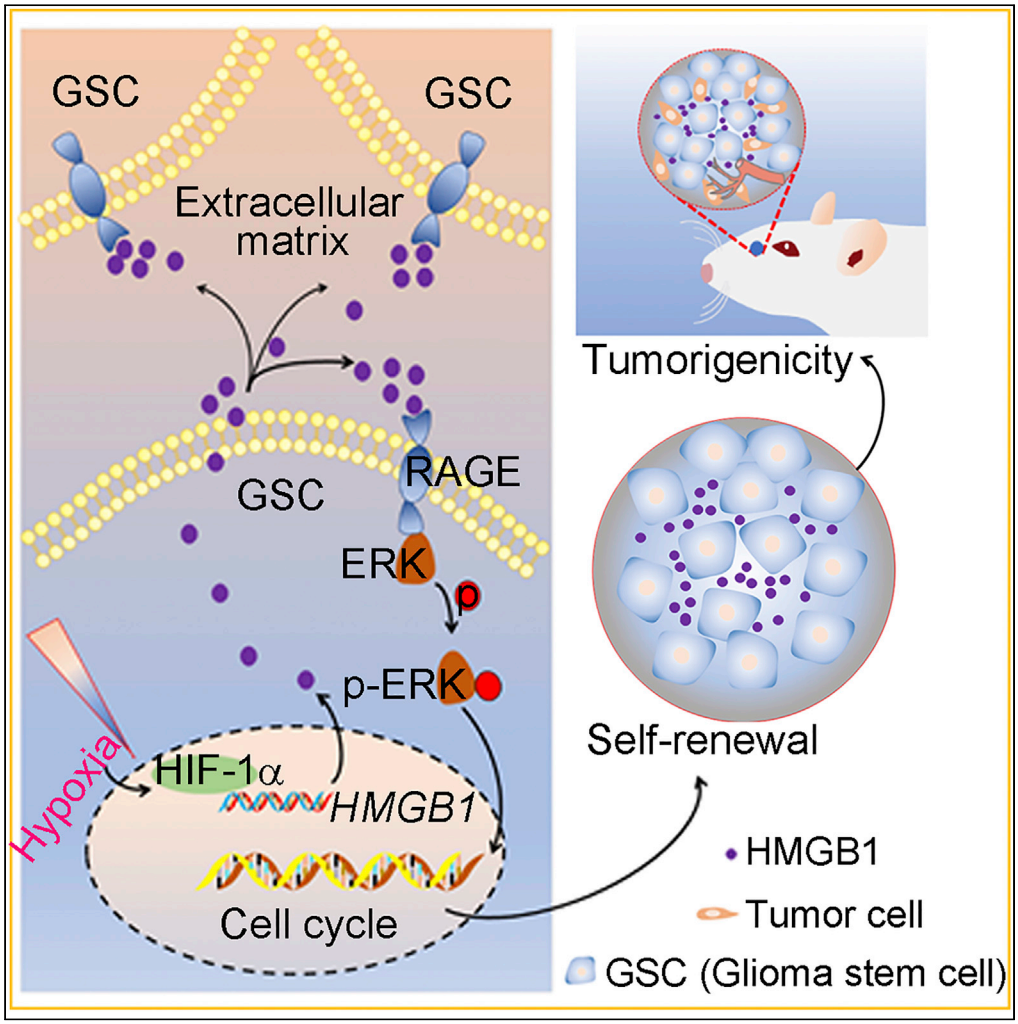

Cuifang Ye, Huan Li, Yachao Li, ..., Qungen Xiao, Li Niu, Xingjiang Yu

yuxingjiang@hust.edu.cn

Highlights

Glioma stem cells overexpress HMGB1 in human glioblastoma

Hypoxia induces the upregulation and release of HMGB1 in glioma stem cells

HMGB1 promotes the self-renewal of glioma stem cells via RAGE

Targeting HMGB1 inhibits the tumorigenesis of glioma stem cells

Ye et al., iScience 25, 104872
September 16, 2022
https://doi.org/10.1016/j.isci.2022.104872

iScience

CellPress
OPEN ACCESS

Article

Hypoxia-induced HMGB1 promotes glioma stem cells self-renewal and tumorigenicity via RAGE

Cuifang Ye,[1] Huan Li,[1] Yachao Li,[1] Yang Zhang,[1] Guohao Liu,[2] Hailong Mi,[1] Honglian Li,[1] Qungen Xiao,[2] Li Niu,[3] and Xingjiang Yu[1,4,*]

SUMMARY

Glioma stem cells (GSCs) in the hypoxic niches contribute to tumor initiation, progression, and recurrence in glioblastoma (GBM). Hypoxia induces release of high-mobility group box 1 (HMGB1) from tumor cells, promoting the development of tumor. Here, we report that HMGB1 is overexpressed in human GBM specimens. Hypoxia promotes the expression and secretion of HMGB1 in GSCs. Furthermore, silencing HMGB1 results in the loss of stem cell markers and a reduction in self-renewal ability of GSCs. Additionally, HMGB1 knockdown inhibits the activation of RAGE-dependent ERK1/2 signaling pathway and arrests the cell cycle in GSCs. Consistently, FPS-ZM1, an inhibitor of RAGE, downregulates HMGB1 expression and the phosphorylation of ERK1/2, leading to a reduction in the proliferation of GSCs. In xenograft mice of GBM, HMGB1 knockdown inhibits tumor growth and promotes mouse survival. Collectively, these findings uncover a vital function for HMGB1 in regulating GSC self-renewal potential and tumorigenicity.

INTRODUCTION

Glioblastoma (GBM) is the most common and aggressive malignant primary brain tumor with poor patient survival (Dumas et al., 2020). GBM is characterized by extensive tissue hypoxia, cellular heterogeneity, as well as cellular hierarchies with stem-like properties. These glioma stem cells (GSCs) can self-renew (Gimple et al., 2019; Man et al., 2014), contributing to tumor malignant progression and difficulty in developing effective therapies. Therefore, elucidating the molecular mechanisms that govern GSC maintenance will provide a better understanding of GBM tumorigenesis.

GSCs are enriched in the protective niches such as tumor necrotic niches (Hambardzumyan and Bergers, 2015) and perivascular niches (Aderetti et al., 2018). Hypoxia is the distinct feature of the GSC niches, which is a critical microenvironment for GSC maintenance (Aderetti et al., 2018; Colwell et al., 2017). Under hypoxia, the immediate adaptive response of GSCs is the activation of hypoxia-inducible factors 1 and 2 (HIF-1 and HIF-2). Such transcription factors control target genes to maintain the self-renewal of GSCs, enhancing their tumorigenic capacity (Heddleston et al., 2009; Huang et al., 2021; Li et al., 2009; Man et al., 2018). Cumulative evidence has demonstrated that hypoxia-induced HIF-1α takes an important part in GBM progression by regulating various processes including maintaining GSCs (Heddleston et al., 2009), angiogenesis (Rong et al., 2006), metabolic reprogramming (Zhang et al., 2021; Gabriely et al., 2017), cell migration (Bao et al., 2018), and therapy resistance (Huang et al., 2019). However, the mechanism of hypoxia maintaining GSCs requires further investigation.

Together with HIFs activation, hypoxia induces the release or secretion of damage-associated molecular patterns (DAMPs) such as high-mobility group box protein 1 (HMGB1) in cancer (Hernandez et al., 2016; Xue et al., 2021). HMGB1 is both a nonhistone nuclear protein and a secreted protein (Bianchi, 2007), playing a pivotal role in inflammation and the proliferation of tumor cells (Cheng et al., 2018; Tang et al., 2010a; Wang and Zhang., 2020). HMGB1 is overexpressed in various solid tumors, promoting tumor progression (Tang et al., 2010a). Accumulating evidence has demonstrated that hypoxia induces tumor cells to actively secrete HMGB1 into extracellular matrix (Cheng et al., 2018; Tsung et al., 2007; Tang et al., 2010b; Yan et al., 2012). Subsequently, extracellular HMGB1 functions as a paracrine/autocrine factor to activate signaling cascades through binding to its receptors such as the receptor for advanced glycation end products (RAGE), Toll-like receptor (TLR) 2, TLR4, and TLR9 (Rapoport et al., 2020; Wu and Yang, 2018; Zhang et al., 2018; He et al., 2018). Importantly, HMGB1 highly expresses in human GBM tissue and is associated

[1]Department of Histology and Embryology, Tongji Medical College, Huazhong University of Science and Technology, Wuhan 430030, P.R. China

[2]Department of Neurosurgery, Tongji Hospital, Tongji Medical College, Huazhong University of Science and Technology, Wuhan 430030, P.R. China

[3]Department of Pathology, Zhongnan Hospital of Wuhan University, Wuhan 430071, P.R. China

[4]Lead contact

*Correspondence: yuxingjiang@hust.edu.cn

https://doi.org/10.1016/j.isci.2022.104872

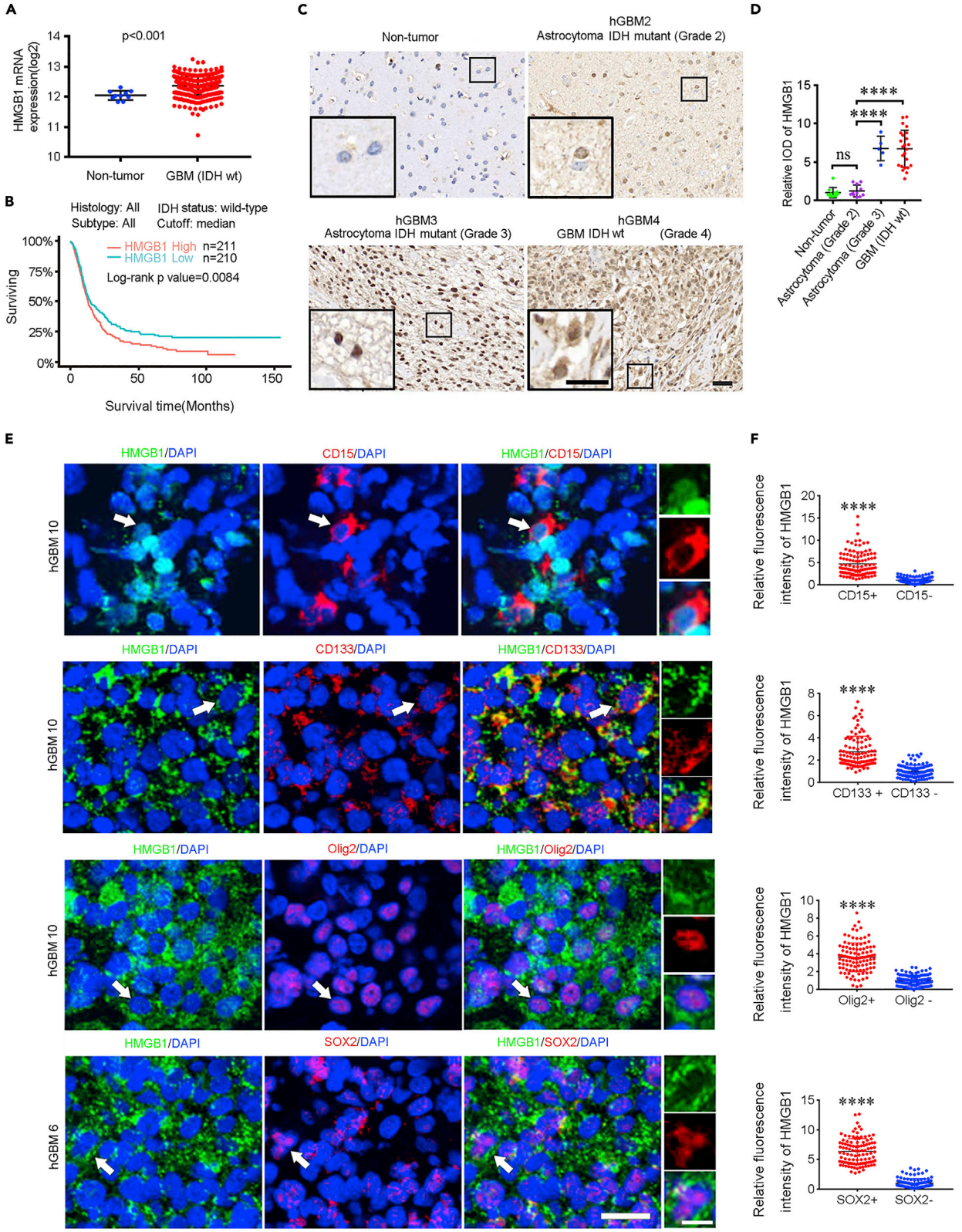
A
p<0.001
HMGB1 mRNA expression(log2)
Non-tumor
GBM (IDH wt)
B
Histology: All
Subtype: All
IDH status: wild-type
Cutoff: median
HMGB1 High n=211
HMGB1 Low n=210
Log-rank p value=0.0084
Surviving
Survival time(Months)
C
Non-tumor
hGBM2
Astrocytoma IDH mutant (Grade 2)
hGBM3
Astrocytoma IDH mutant (Grade 3)
hGBM4
GBM IDH wt (Grade 4)
D
Relative IOD of HMGB1
ns
****
Non-tumor
Astrocytoma (Grade 2)
Astrocytoma (Grade 3)
GBM (IDH wt)
E
HMGB1/DAPI
CD15/DAPI
HMGB1/CD15/DAPI
hGBM 10
CD133/DAPI
HMGB1/CD133/DAPI
Olig2/DAPI
HMGB1/Olig2/DAPI
SOX2/DAPI
HMGB1/SOX2/DAPI
hGBM 6
F
Relative fluorescence intensity of HMGB1
CD15+
CD15-
CD133 +
CD133 -
Olig2+
Olig2 -
SOX2+
SOX2-

Figure 1. HMGB1 correlates with glioma aggressiveness and is elevated in GSCs

(A) HMGB1 mRNA expression in normal brain (n = 10) and glioblastoma (GBM, IDH wild-type, n = 528) from the TCGA database. Significance was determined by Mann-Whitney U test. wt, wild-type.

(B) Kaplan-Meier survival analysis of patients with gliomas with IDH wild type stratified by HMGB1 expression from the CGGA database. Median HMGB1 expression was used for stratification into HMGB1 high and HMGB1 low groups.

(C and D) Immunohistochemistry (IHC) staining of HMGB1 in human normal brain and different grade of gliomas. (C) The corresponding enlarged image of the rectangular box is in the lower left. Representative images are shown. Scale bar, 50 μm. (D) Quantitative analysis of HMGB1 expression in human normal brain and gliomas. HMGB1 immunostaining intensity was assessed by the Integrated Optical Density (IOD, area × mean optical density). Data are normalized to non-tumor group and represented as mean ± SD Significance was analyzed by one-way ANOVA with Tukey's test. Non-tumor, n = 11; astrocytoma (IDH mutant, Grade 2), n = 11; astrocytoma (IDH mutant, Grade 3), n = 5; GBM (IDH wt), n = 24. ns, no significance; ****, $p < 0.0001$.

(E and F) Immunofluorescent double staining of HMGB1 (green) and stem cell markers (CD15, CD133, SOX2, or Olig2; red) in human GBM specimens. DAPI stained nuclei (blue). (E) Representative images are shown. Arrows show the cells in which HMGB1 and stem cell marker are co-expressed. Scale bar, 25μm. The zoom-in images are on the right. Scale bar, 10μm. (F) Quantitative analysis of HMGB1 immunoreactivity in stem cell marker positive (+) or negative (−) cells. Data are normalized to the group of stem cell marker negative cells and represented as mean ± SD Each dot represents a single cell, n = 106 total cells from three human GBM specimens (20–50 cells from each specimen). Significance was determined by Mann-Whitney U test. ****, $p < 0.0001$.

See also Figure S1.

with poor prognosis (Cheng et al., 2018; Wang et al., 2015; Zhao et al., 2021). The interaction of HMGB1 and RAGE contributes to the accelerated growth of gliomas in diabetes mice (Zhang et al., 2020). HMGB1 promotes the phenotype of cancer stem-like cells in several types of cancer including lung, colon, and pancreatic cancer (Zhao et al., 2017; Qian et al., 2019; Zhang et al., 2019a). Temozolomide treatment induces the upregulation of HMGB1 in biopsy-derived GBM cells, which promotes the formation of GSCs via TLR2 (Gao et al., 2021). In addition, hypoxia also upregulates the expression of DAMPs receptors (Russo et al., 2015; Rider et al., 2012). It has been reported that RAGE expression is upregulated with the increase of HIF-1α expression in both GBM tumor tissue and cell lines (Tafani et al., 2011). Hence, we speculate that HMGB1 might be linked with GBM progression by promoting GSCs growth under hypoxia.

In this study, we demonstrate that hypoxia elevates HMGB1 expression and promotes HMGB1 release from GSCs. HMGB1 knockdown inhibits cell proliferation and impairs the phenotype of GSCs via inhibiting RAGE-dependent ERK1/2 signaling pathway. GSCs expressing HMGB1 shRNA exhibit reduced tumorigenicity in xenografts. These results indicate that HMGB1 could act as a candidate therapeutic target for exploring new therapeutic strategies in GBM.

RESULTS

HMGB1 correlates with glioma aggressiveness and is elevated in glioma stem cells

Patients with glioma with isocitrate dehydrogenase (IDH) wild type (wt) have a worse prognosis than patients with IDH mutation (Eckel-Passow et al., 2015). To investigate the role of HMGB1 in the tumor progression of GBM (IDH wt, Grade 4), we first queried The Cancer Genome Atlas (TCGA) and Chinese Glioma Genome Atlas (CGGA) from GlioVis (http://gliovis.bioinfo.cnio.es/). HMGB1 expression was significantly upregulated in GBM (IDH wt) compared to normal brain tissue (Figure 1A). The CGGA database showed that HMGB1 expression correlated with poor patient survival in gliomas with IDH wt (Figure 1B). Subset analysis of HMGB1 expression in GBM with IDH wt was not of prognostic significance (not shown). We next performed immunohistochemical analysis to examine HMGB1 expression in human glioma tissue arrays including Grade 2 (n = 11) and Grade 3 (n = 5) astrocytoma with IDH mutant, GBM with IDH wt (n = 24), and normal brain tissue (n = 11). Normal brain tissue showed weak staining of HMGB1 (Figures 1C and 1D). In contrast, glioma specimens, especially, Grade 3 astrocytoma and GBM exhibited higher expression of HMGB1 (Figures 1C and 1D). More importantly, HMGB1 mainly localized in the nuclei of focal tumor cells in Grade 2 and Grade 3 astrocytomas. However, in addition to nuclear HMGB1, cytoplasmic HMGB1 was also present in most GBM specimens (Figure 1C). These data suggest that HMGB1 expression is significantly elevated in more aggressive glioma.

In addition, the CGGA database showed that the levels of HMGB1 highly correlated with the expression of tumor stem cell markers including SOX2, Olig2, FUT4 (CD15), PROM1 (CD133), and CD44 in GBM (IDH wt) (Figure S1A). Next, we identified the expression of HMGB1 in stem cell marker–positive cells. Both cytoplasmic and nuclear HMGB1 immunoreactivity were positive in CD15, CD133, Olig2, or SOX2-positive cells (Figures 1E and S1B). Quantitative analysis demonstrated that HMGB1 was highly expressed in stem cell marker–positive cells (Figure 1F). Collectively, these results suggest that GSCs highly express HMGB1 in human GBM.

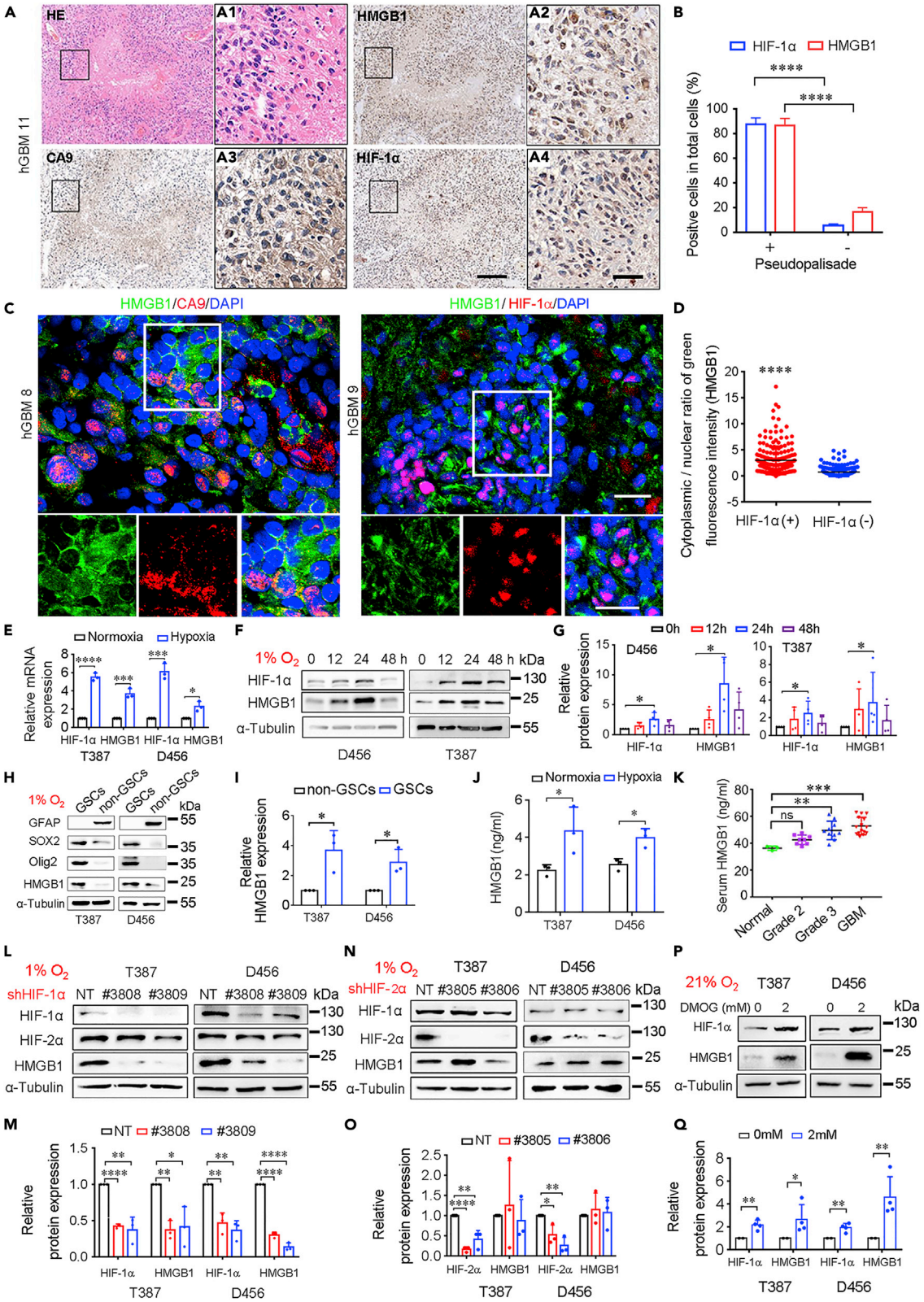
A
HE
A1
HMGB1
A2
hGBM 11
CA9
A3
HIF-1α
A4
B
HIF-1α HMGB1
****
****
Positive cells in total cells (%)
100
80
60
40
20
0
+
-
Pseudopalisade
C
HMGB1/CA9/DAPI
HMGB1/ HIF-1α/DAPI
hGBM 8
hGBM 9
D
****
Cytoplasmic / nuclear ratio of green fluorescence intensity (HMGB1)
20
15
10
5
0
-5
HIF-1α (+)
HIF-1α (-)
E
Normoxia
Hypoxia
Relative mRNA expression
****
***
***
*
HIF-1α HMGB1 HIF-1α HMGB1
T387
D456
F
1% O2
0 12 24 48 h 0 12 24 48 h kDa
HIF-1α
HMGB1
α-Tubulin
130
25
55
D456
T387
G
0h 12h 24h 48h
Relative protein expression
D456
T387
HIF-1α
HMGB1
HIF-1α
HMGB1
H
1% O2
GSCs non-GSCs GSCs non-GSCs kDa
GFAP
SOX2
Olig2
HMGB1
α-Tubulin
55
35
35
25
55
T387
D456
I
non-GSCs GSCs
Relative HMGB1 expression
T387
D456
J
Normoxia Hypoxia
HMGB1 (ng/ml)
T387
D456
K
***
**
ns
Serum HMGB1 (ng/ml)
Normal
Grade 2
Grade 3
GBM
L
1% O2
T387
D456
shHIF-1α NT #3808 #3809 NT #3808 #3809 kDa
HIF-1α
HIF-2α
HMGB1
α-Tubulin
130
130
25
55
N
1% O2
T387
D456
shHIF-2α NT #3805 #3806 NT #3805 #3806 kDa
HIF-1α
HIF-2α
HMGB1
α-Tubulin
130
130
25
55
P
21% O2
T387
D456
DMOG (mM) 0 2 0 2 kDa
HIF-1α
HMGB1
α-Tubulin
130
25
55
M
NT #3808 #3809
Relative protein expression
HIF-1α HMGB1 HIF-1α HMGB1
T387
D456
O
NT #3805 #3806
Relative protein expression
HIF-2α HMGB1 HIF-2α HMGB1
T387
D456
Q
0mM 2mM
Relative protein expression
HIF-1α HMGB1 HIF-1α HMGB1
T387
D456

Figure 2. Hypoxia induces the expression and release of HMGB1 in GSCs

(A and B) HE staining and IHC staining of HMGB1 and hypoxia markers (CA9 or HIF-1α) in the serial sections of human GBM specimen. (A) Representative images are shown. Rectangular boxes show the pseudopalisades surrounding tumor necrosis foci. Scale bar, 200 μm. (A1) – (A4) The zoom-in images of the rectangular box in corresponding left images. Representative images are shown. Scale bar, 50μm. (B) Quantitative analysis of the percentage of HMGB1 or HIF-1α positive cells within (+) or beyond (−) the pseudopalisades. Data are represented as mean ± SD Significance was determined by two-tailed unpaired Student's *t* test. n = 10 high-powered fields. ****, $p < 0.0001$.

(C and D) Immunofluorescent double staining of HMGB1 (green) and hypoxia markers (CA9 or HIF-1α, red) in human GBM specimens. DAPI stained nuclei (blue). (C) The enlarged images of the rectangular box are in the lower panel. Representative images of GBM specimens are shown. Scale bar, 25 μm. (D) Quantitative analysis of cytoplasmic/nuclear ratio of HMGB1 expression in HIF-1α positive (+) or negative (−) cells. Data are normalized to the fluorescence intensity of HIF-1α negative cells and represented as mean ± SD Each dot represents a single cell, n = 205 total cells from three human GBM specimens (50–70 cells from each specimen). Significance was determined by Mann-Whitney U test. ****, $p < 0.0001$.

(E) qPCR analysis of HMGB1 and HIF-1α mRNA levels in GSCs cultured under standard conditions (normoxia, 21% O_2) or hypoxia (1% O_2) for 24 h. Data are normalized to normoxia group and represented as mean ± SD Significance was determined by two-tailed unpaired Student's *t* test. n = 3 replicates for each group. *, $p < 0.05$; ***, $p < 0.001$; ****, $p < 0.0001$.

(F and G) Western blot and quantitative analysis of HMGB1 and HIF-1α protein expression in GSCs cultured under hypoxia for different hours. (F) Representative blots are shown. (G) Data are normalized to 0 h group and represented as mean ± SD Significance was determined by Mann-Whitney U test. n = 4 replicates for each group. *, $p < 0.05$.

(H and I) Western blot and quantitative analysis of HMGB1 protein expression in matched GSCs and non-GSCs under hypoxia for 24 h. (H) Representative blots are shown. (I) Data are normalized to non-GSCs group and represented as mean ± SD Significance was determined by two-tailed unpaired Student's *t* test. n = 3 replicates for each group. *, $p < 0.05$.

(J) ELISA analysis of HMGB1 in the medium supernatant of GSCs under normoxia or hypoxia for 72 h. Data are represented as mean ± SD Significance was determined by two-tailed unpaired Student's *t* test. *, $p < 0.05$.

(K) ELISA analysis of HMGB1 in the serum of normal population and human glioma patients before surgery. Data are represented as mean ± SD Significance was analyzed by one-way ANOVA with Tukey's test. Normal population, n = 3; astrocytoma (IDH mutant, Grade 2), n = 8; astrocytoma (IDH mutant, Grade 3), n = 10; GBM (IDH wild-type), n = 15. ns, no significance; **, $p < 0.01$; ***, $p < 0.001$.

(L and M) Western blot and quantitative analysis of HMGB1 and HIF-1α protein expression in GSCs with HIF-1α knockdown under hypoxia for 24 h. (L) Representative blots are shown. #3808 and #3809, two different shHIF-1α sequences. (M) Data are normalized to shNT group and represented as mean ± SD NT, nontargeting sequence. Significance was determined by two-tailed unpaired Student's *t* test. n = 3 replicates for each group. *, $p < 0.05$; **, $p < 0.01$; ****, $p < 0.0001$.

(N and O) Western blot and quantitative analysis of HMGB1 and HIF-2α protein expression in GSCs with HIF-2α knockdown under hypoxia for 24 h. (N) Representative blots are shown. #3805 and #3806, two different shHIF-2α sequences. (O) Data are normalized to shNT group and represented as mean ± SD Significance was determined by two-tailed unpaired Student's *t* test. n = 3 replicates for each group. *, $p < 0.05$; **, $p < 0.01$; ****, $p < 0.0001$.

(P and Q) Western blot and quantitative analysis of HIF-1α and HMGB1 in GSCs treated with DMOG for 48 h under normoxia. (P) Representative blots are shown. (Q) Data are normalized to 0 mM DMOG group (DMSO treatment) and represented as mean ± SD Significance was determined by two-tailed unpaired Student's *t* test. n = 4 replicates for each group. *, $p < 0.05$; **, $p < 0.01$.

See also Figure S2.

Hypoxia induces the overexpression and release of HMGB1 in glioma stem cells

Given that GSCs are enriched in tumor hypoxic niches, we determined whether the upregulation of HMGB1 is induced by hypoxia. The CGGA database showed that the HMGB1 mRNA levels correlated with the levels of multiple hypoxia response genes including HIF-1α, CA9, VEGFA, HK2, and LDHA in GBM (IDH wt) (Figure S2A). Immunohistochemical analyses showed that intense HMGB1 immunoreactivity was present in both nuclei and cytoplasm of tumor cells in the pseudopalisades surrounding tumor necrosis foci in human GBM specimens (Figure 2A). Quantitative analysis further demonstrated that there were more HIF-1α-positive cells in the pseudopalisades. The percentage of HMGB1 positive cells was also increased in these pseudopalisades (Figure 2B).

Consistently, immunofluorescent double staining confirmed that HMGB1 was expressed in CA9 or HIF-1α-positive tumor cells (Figures 2C and S2B). Quantitative analysis showed that the cytoplasmic to nuclear ratio of HMGB1 expression was higher in HIF-1α positive cells than that in HIF-1α negative cells (Figure 2D). It has been reported that cytoplasmic HMGB1 expression is associated with its secretion or release (Jube et al., 2012; Yan et al., 2012). Together, these data suggest that enhanced HMGB1 expression may be associated with hypoxia in GBM.

To further verify the influence of hypoxia on HMGB1 expression, human GSC lines (D456 and T387) were subjected to hypoxic culture for different time. Compared to normoxia (0 h), HIF-1α and HMGB1 expression was markedly upregulated in GSCs under hypoxia (1% O_2) for 24 h (Figures 2E–2G). At the same time, we tested HMGB1 expression in GSC lines and matched non-GSCs derived from the same tumors. The non-GSCs were obtained, as previously described (Man et al., 2018). We identified GSCs and non-GSCs by detecting the expression of stem cell markers such as Olig2 and SOX2 or the expression of differentiation

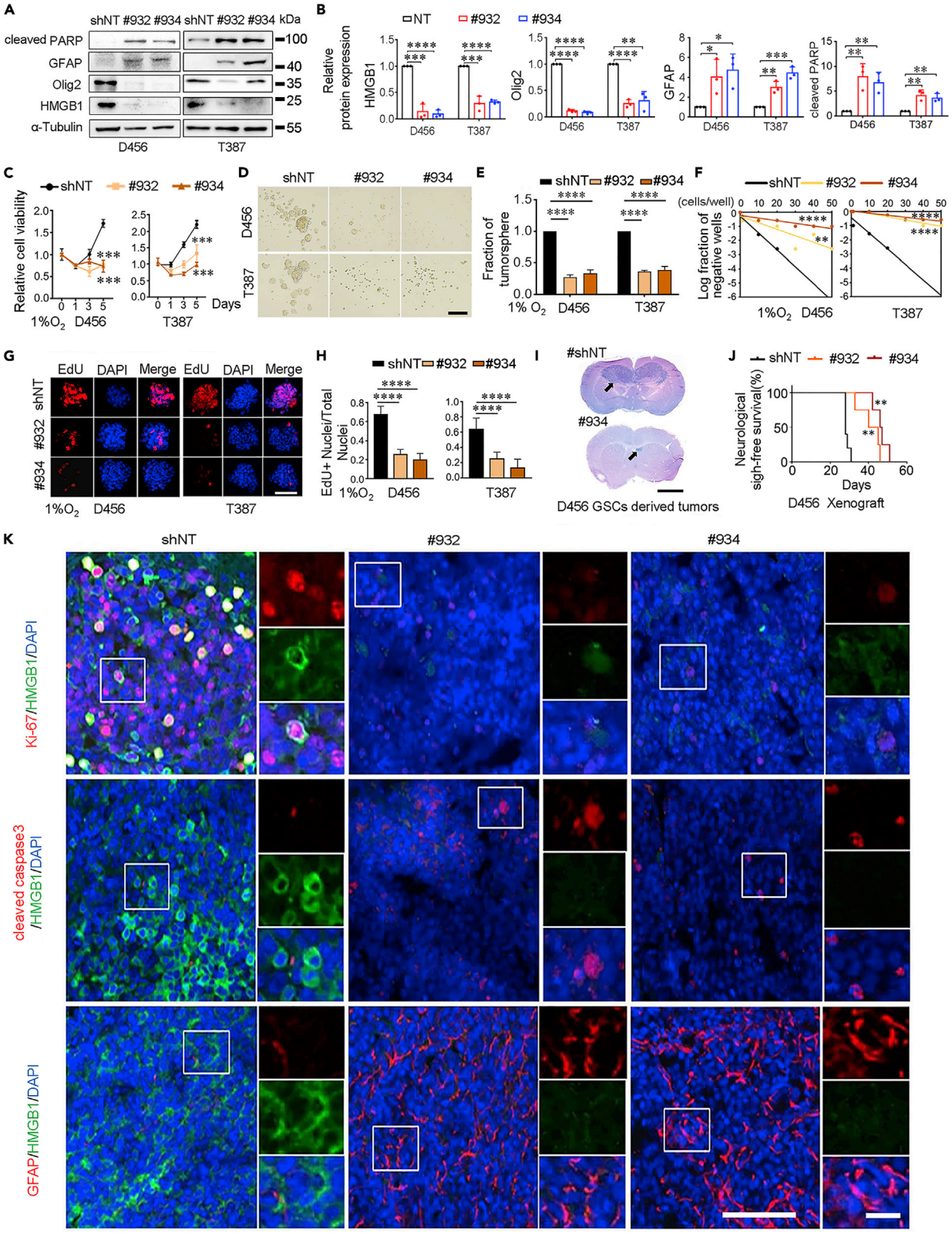
A
shNT #932 #934 shNT #932 #934 kDa
cleaved PARP
GFAP
Olig2
HMGB1
α-Tubulin
100
40
35
25
55
D456
T387
B
NT
#932
#934
Relative protein expression
HMGB1
Olig2
GFAP
cleaved PARP
D456
T387
C
shNT
#932
#934
Relative cell viability
1%O2 D456
T387
Days
D
shNT
#932
#934
D456
T387
E
shNT
#932
#934
Fraction of tumorsphere
1% O2 D456
T387
F
shNT
#932
#934
(cells/well)
Log fraction of negative wells
1%O2 D456
T387
G
EdU DAPI Merge EdU DAPI Merge
shNT
#932
#934
1%O2 D456
T387
H
shNT
#932
#934
EdU+ Nuclei/Total Nuclei
1%O2 D456
T387
I
#shNT
#934
D456 GSCs derived tumors
J
shNT
#932
#934
Neurological sigh-free survival(%)
Days
D456 Xenograft
K
shNT
#932
#934
Ki-67/HMGB1/DAPI
cleaved caspase3 /HMGB1/DAPI
GFAP/HMGB1/DAPI

Figure 3. HMGB1 promotes the proliferation and tumorigenesis of GSCs

(A and B) Western blot and quantitative analysis of HMGB1, Olig2, GFAP, and cleaved PARP expression in GSCs with shNT or shHMGB1 under hypoxia for 24 h. (A) Representative blots are shown. (B) Data are normalized to shNT group and represented as mean ± SD NT, nontargeting sequence. #932 and #934, two different shHMGB1 sequences. Significance was determined by two-tailed unpaired Student's *t* test. n = 3 replicates for each group.*, $p < 0.05$; **, $p < 0.01$; ***, $p < 0.001$; ****, $p < 0.0001$.

(C) Cell viability of GSCs under hypoxia for different days (0, 1, 3, and 5). Data are normalized to 0 days group and represented as mean ± SD Significance was determined by two-tailed unpaired Student's *t* test. n = 3 replicates for each group. ***, $p < 0.001$, compared to shNT group.

(D and E) Tumorsphere formation analysis of GSCs with shHMGB1 under hypoxia for 7 days. (D) Representative images are shown. Scale bar, 200 μm.

(E) Quantitative analysis of tumorsphere number. Data are normalized to shNT group and represented as mean ± SD Significance was determined by two-tailed unpaired Student's *t* test. n = 3 replicates for each group. ****, $p < 0.0001$.

(F) *In vitro* limiting dilution assay of GSCs under hypoxia for 7 days **, $p < 0.01$; ****, $p < 0.0001$, compared to shNT group. n = 3 replicates for each group.

(G and H) Fluorescent images and quantitative analysis of EdU incorporation in GSC tumorsphere under hypoxia for 24 h. (G) Representative images are shown. Scale bar, 50 μm. (H) Quantitative analysis of EdU positive (+) cells. Data are represented as mean ± SD Significance was determined by two-tailed unpaired Student's *t* test. n = 3 replicates for each group. ****, $p < 0.0001$.

(I) Hematoxylin and eosin (HE) staining of xenograft mice brains at 28 days after transplantation. Representative images are shown. Arrows show the tumors. Scale bar, 10 mm.

(J) Kaplan-Meier survival curve of mice implanted with D456 GSCs expressing shNT or shHMGB1. Significance was analyzed by using Log rank test. n = 5 for each group. **, $p < 0.01$, compared to shNT mice.

(K) Immunofluorescent staining of HMGB1 (green), Ki67 (red), cleaved caspase3 (red), or GFAP (red) in GBM xenograft mice. DAPI stained the nuclei (blue). Scale bar, 100μm. The zoom-in images of rectangle images are on the right. Representative images are shown. Scale bar, 25μm.

See also Figure S3.

marker GFAP. Different from GSCs, non-GSCs could highly express GFAP (Figures 2H and 2I). After hypoxia treatment, both of GSC lines displayed a higher level of HMGB1 than their counterpart non-GSCs (Figures 2H and 2I). Moreover, both cytoplasmic and nuclear HMGB1 levels were also higher in GSCs than that in non-GSCs under normoxia (Figures S2C and S2D). More importantly, hypoxia significantly increased HMGB1 concentration in the medium supernatant of GSCs (Figure 2J). Consistently, patients with glioma before surgery, especially patients with GBM (IDH wt) showed higher levels of serum HMGB1 than normal population (Figure 2K).

Since the HIF proteins act as one of the key regulators that maintains the phenotype of GSCs in the hypoxic microenvironment, we then examined whether HIFs regulate HMGB1 expression in GSCs under hypoxia. We silenced HIF-1α or HIF-2α using two different, non-overlapping small hairpin RNA (shRNA) sequences. Knockdown of HIF-1α, but not HIF-2α, vividly diminished HMGB1 expression under hypoxic conditions, indicating that HIF-1α is involved in regulating HMGB1 expression in GSCs (Figures 2L–2O). Consistently, treatment with dimethyloxalylglycine (DMOG), a HIF-1α stabilizer, significantly upregulated the protein levels of both HIF-1α and HMGB1 under normoxia for 48 h (Figures 2P and 2Q). Collectively, these data reveal that HMGB1 is preferentially induced by hypoxia in GSCs.

HMGB1 promotes self-renewal and tumorigenesis of GSCs

Hypoxia serves as a key microenvironment for maintaining GSC stemness and their functional characteristics (Seidel et al., 2010; Soeda et al., 2009). Hence, we examined whether hypoxia-induced HMGB1 contributes to the survival and self-renewal capacity of GSCs. HMGB1 knockdown resulted in reduced expression of stem cell marker Olig2 and increased expression of differentiation marker GFAP (Figures 3A, 3B and S3A). These cells exhibited an increase in the expression of cleaved PARP (Figures 3A and 3B). Cell viability was reduced in GSCs with HMGB1 knockdown (Figure 3C). Deletion of HMGB1 noticeably inhibited the tumorsphere formation ability of GSCs (D456 and T387) under hypoxic conditions, as assessed by tumorsphere formation assay (Figures 3D and 3E). In addition, tumorsphere number of GSCs with shHMGB1 was ~50% of that of GSCs with shNT under normoxic conditions (Figure S3B). *In vitro* limiting dilution assay also confirmed that silencing of HMGB1 resulted in declined self-renewal capacity of GSCs under hypoxia (Figure 3F). EdU staining assays proved that the loss of HMGB1 impaired the proliferation of GSCs subjected to hypoxia (Figures 3G and 3H). Together, these data imply that HMGB1 is a crucial factor in regulating GSCs characteristics under hypoxia.

To further demonstrate the role of HMGB1 in the tumorigenicity of GSCs, we established orthotopic xenografts using D456 GSCs expressing either nontargeting shRNA (shNT) or HMGB1 shRNA (shHMGB1). After 28 days, the shNT mice firstly developed neurologic signs, whereas shHMGB1 mice were clinically asymptomatic. For evaluating tumor formation, a subset of mice in each group was sacrificed for histologic analysis at 28 days after implantation. Hematoxylin and eosin (HE) staining showed that the tumors in shNT mice

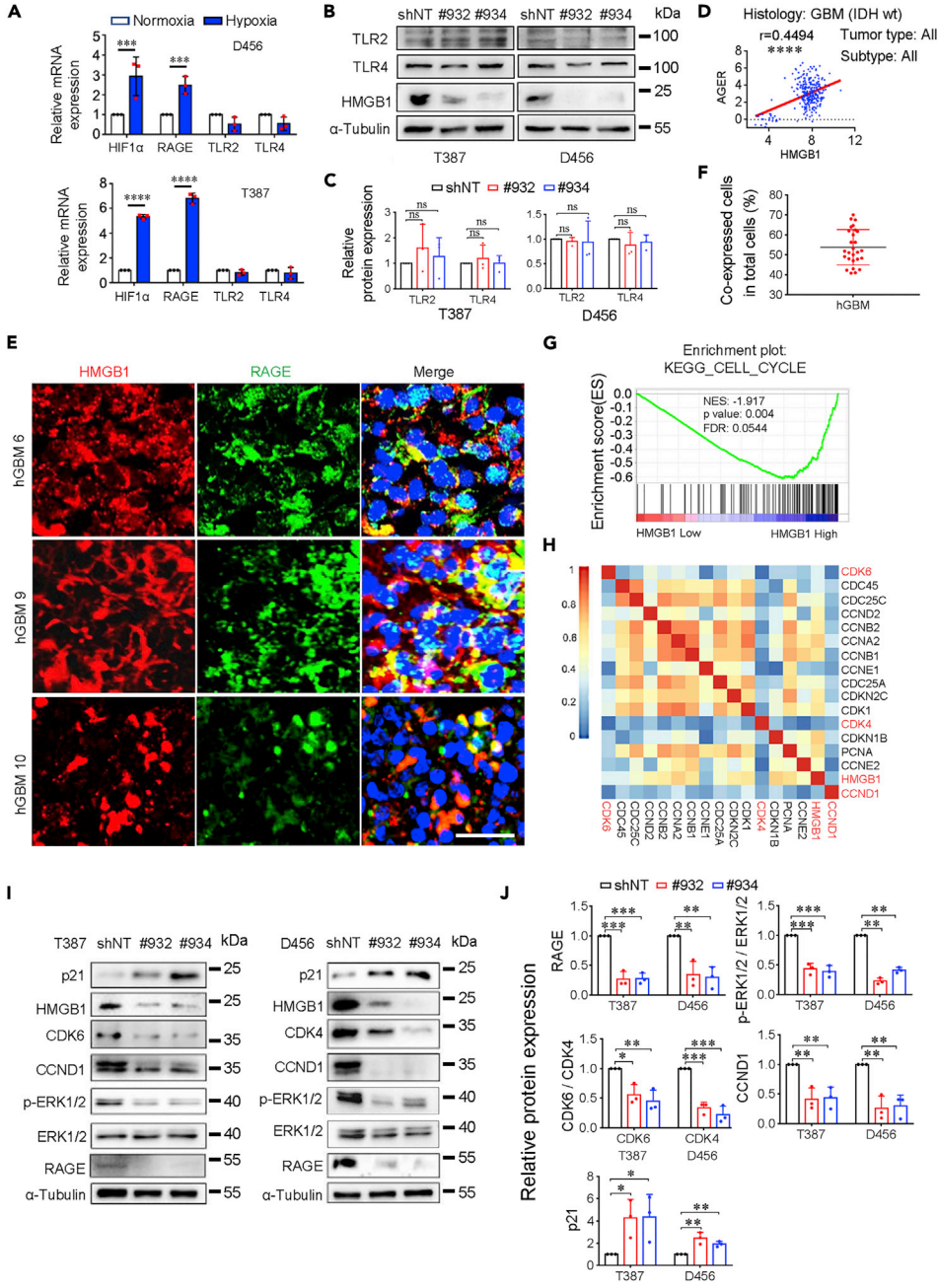

Figure 4. HMGB1 promotes cell cycle progression via RAGE-dependent ERK1/2 signaling pathway in GSCs

(A) qPCR analysis of RAGE, TLR2, and TLR4 mRNA levels in GSCs under hypoxia for 24 h. Data are normalized to normoxia group and represented as mean ± SD Significance was determined by two-tailed unpaired Student's *t* test. n = 3 replicates for each group. ***, $p < 0.001$; ****, $p < 0.0001$.

(B and C) Western blot and quantitative analysis of TLR2 and TLR4 expression in GSCs with HMGB1 knockdown under hypoxia for 24 h. (B) Representative blots are shown. (C) Data are normalized to shNT group and represented as mean ± SD Significance was determined by two-tailed unpaired Student's *t* test. n = 3 replicates for each group. ns, no significance.

(D) The correlation of HMGB1 mRNA expression with AGER (RAGE mRNA) in patients with GBM (IDH wt) from CGGA database using Pearson's correlation analysis. n = 288, r = 0.4494; ****, $p < 0.0001$.

(E and F) Immunofluorescent double staining of HMGB1 (red) and RAGE (green) in human GBM specimens. DAPI stained nuclei (blue). (E) Representative images are shown. Scale bar, 25μm. (F) Quantitative analysis of cells co-expressing HMGB1 and RAGE in total cells. Data are represented as mean ± SD 9 random microscope fields of each GBM specimen (n = 3) were selected.

Figure 4. *Continued*
(G and H) GSEA and heatmap show upregulation of cell cycle progression genes in patients with GBM with higher expression of HMGB1 based on the CGGA dataset. NES, normalized enrichment score. FDR, false discovery rate.
(I and J) Western blot and quantitative analysis of the expression of RAGE-dependent ERK1/2 signaling molecules in GSCs with HMGB1 knockdown under hypoxia for 24 h. (I) Representative blots are shown. (J) Data are normalized to shNT group and represented as mean ± SD Significance was determined by two-tailed unpaired Student's *t* test. n = 3 replicates for each group. *, $p < 0.05$; **, $p < 0.01$; ***, $p < 0.001$.

extended to both hemispheres (Figure 3I). However, the shHMGB1 mice developed smaller tumors (Figure 3I). Survival analysis demonstrated that the shHMGB1 mice survived longer than the shNT mice (Figure 3J). HMGB1-immunoreactive products were predominant in the cytoplasm of tumor cells and were faintly detectable in the nuclei in the tumor specimens of shNT xenografts (Figure 3K). HMGB1 was weakly detectable in shHMGB1 mice (Figure 3K). To evaluate the proliferation activity of GSCs in xenografts, immunofluorescent staining was used to detect cycle-specific antigens such as Ki-67. Loss of HMGB1 considerably inhibited the expression of Ki-67, suggesting that the proliferation of GSCs declines in shHMGB1 xenografts (Figure 3K). Compared with shNT mice, shHMGB1 mice specimens showed an increase in the expression of cleaved caspase-3 and GFAP (Figure 3K), which was consistent with the results *in vitro*. In general, these data indicate that HMGB1 plays a vital role in regulating the self-renewal of GSCs and promoting the tumorigenicity of GSCs.

HMGB1 accelerates cell cycle progression through RAGE-dependent ERK1/2 signaling pathway in GSCs

Extracellular HMGB1 functions as a signaling molecule and binds to several receptors including RAGE, TLR2, and TLR4, which further triggers pleiotropic effects including cell proliferation (Huang et al., 2018). Firstly, we assessed the effect of hypoxia on the expression of RAGE, TLR2, and TLR4 in GSCs. Hypoxia strikingly augmented RAGE mRNA levels in GSCs, whereas it had no significant effect on the mRNA levels of TLR2 and TLR4 (Figure 4A). In addition, the silence of HMGB1 did not alter the protein expression of TLR2 and TLR4 in hypoxic GSCs (Figures 4B and 4C). The CGGA dataset showed that the HMGB1 mRNA level was positively correlated with the AGER (RAGE mRNA) level in patients with GBM (IDH wt) (Figure 4D). Immunofluorescent double staining showed that (54 ± 8.7) % of tumor cells co-expressed RAGE and HMGB1 in human GBM specimens (Figures 4E and 4F).

Next, GSEA and KEGG pathway enrichment analyses were used to assay the related functional pathway for HMGB1 affecting GBM progression. We used the median level of HMGB1 expression to classify the patients with GBM with IDH wt into low- and high-expression groups (95 samples for each group) based on clinical data from the CGGA dataset. The analysis indicated that the cell cycle pathway was the most relevant (Figure 4G). Moreover, HMGB1 was highly correlated with cyclin D1 (CCND1), cyclin-dependent kinases 4 and 6 (CDK4 and CDK6), and other molecules in the cell cycle pathway (Figure 4H). Accumulating evidence indicates that the extracellular signal-related kinase (ERK) signaling pathway promotes tumor cell growth and proliferation through targeting CCND complexes with CDK4 and CDK6 in many cancers (Wakimoto et al., 2017; Bahrami et al., 2018). CDK4 and CDK6 are of great significance to allow cell cycle progression from G1 phase into S phase (Crozier et al., 2022). Besides, HMGB1 was reported to activate ERK signaling pathway and regulate tumor cell proliferation via RAGE in gastric cancer and colorectal cancer (Tang et al., 2021; Huang et al., 2018). Hence, we speculated that RAGE-dependent ERK signaling pathway may be involved in the regulation of HMGB1 on GSC proliferation. As expected, knockdown of HMGB1 significantly lessened RAGE protein expression in GSCs subjected to hypoxia (Figures 4I and 4J). However, these data indicate that RAGE could be very important for HMGB1 regulating the self-renewal of GSCs. Furthermore, HMGB1 knockdown significantly moderated the levels of ERK1/2 phosphorylation in GSCs subjected to hypoxia (Figures 4I and 4J). Correspondingly, the expression of both CCND1 and CDK4 or CDK6 was significantly downregulated in GSCs subjected to hypoxia (Figures 4I and 4J). The expression of CDK inhibitor p21 was elevated in GSCs expressing shHMGB1 (Figures 4I and 4J), resulting in cell cycle block.

Consistent with the *in vitro* results, deficiency of HMGB1 diminished RAGE expression and inhibited activation of ERK1/2 signaling pathway in D456 GSC-derived xenografts (Figure 5). Correspondingly, these shHMGB1 mice exhibited reduced expression of CCND1 and CDK4 and enhanced expression of p21 (Figure 5). Collectively, these results reveal that hypoxia-induced HMGB1 activates RAGE-dependent ERK1/2 signaling pathway and upholds the proliferation of GSCs through promoting cell cycle progression.

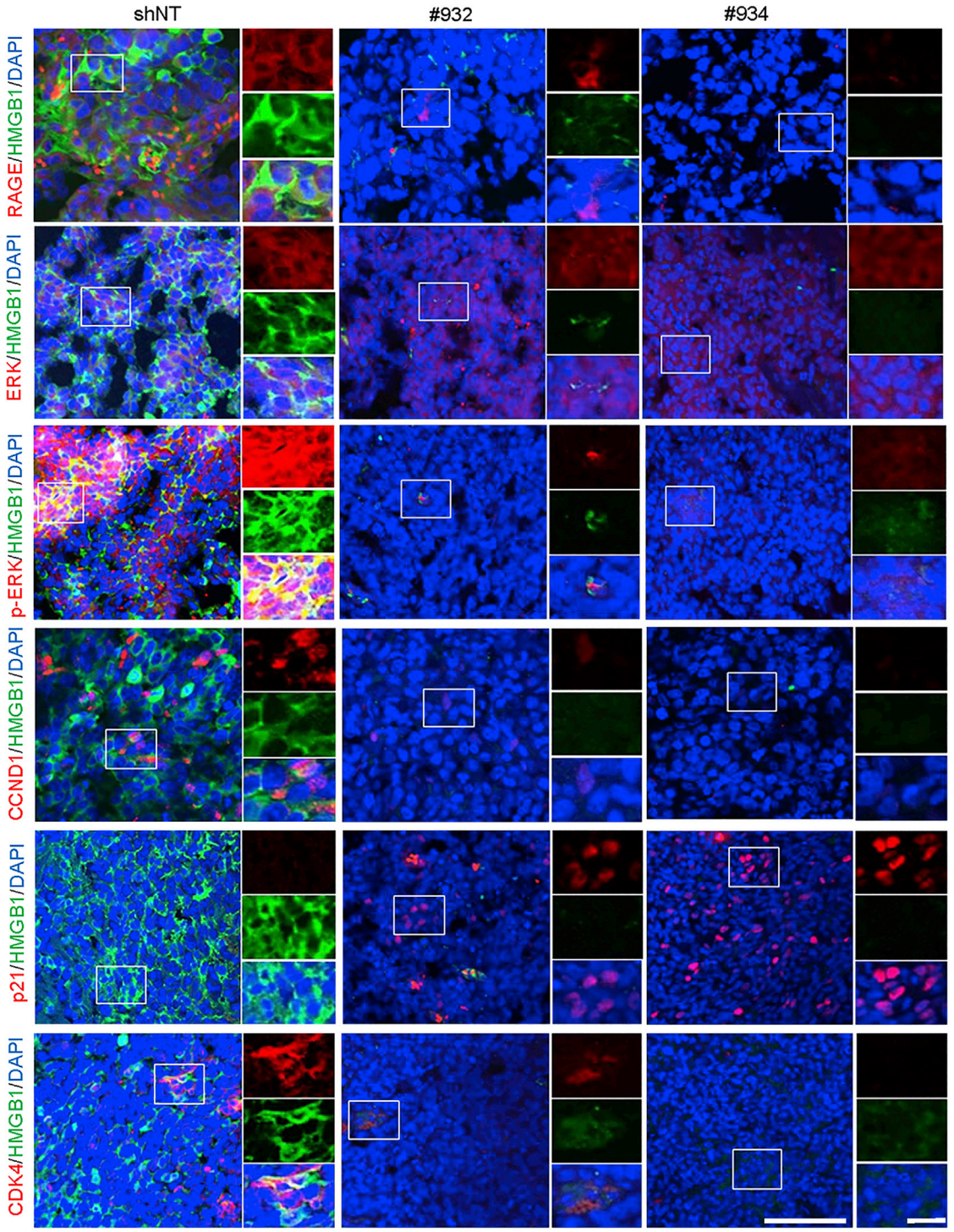

Figure 5. Xenograft mice derived from GSCs expressing shHMGB1 exhibit the inhibition of RAGE-dependent ERK1/2 signaling pathway

Immunofluorescent double staining of HMGB1 (green) and RAGE, ERK1/2, phosphorylated ERK1/2 (*p*-ERK1/2), CCND1, CDK4, or p21 (red) in GBM xenograft mouse tumors. DAPI stained the nuclei (blue). Scale bar, 100 μm. The zoom-in images of rectangle images are on the right. Representative images are shown. Scale bar, 25 μm.

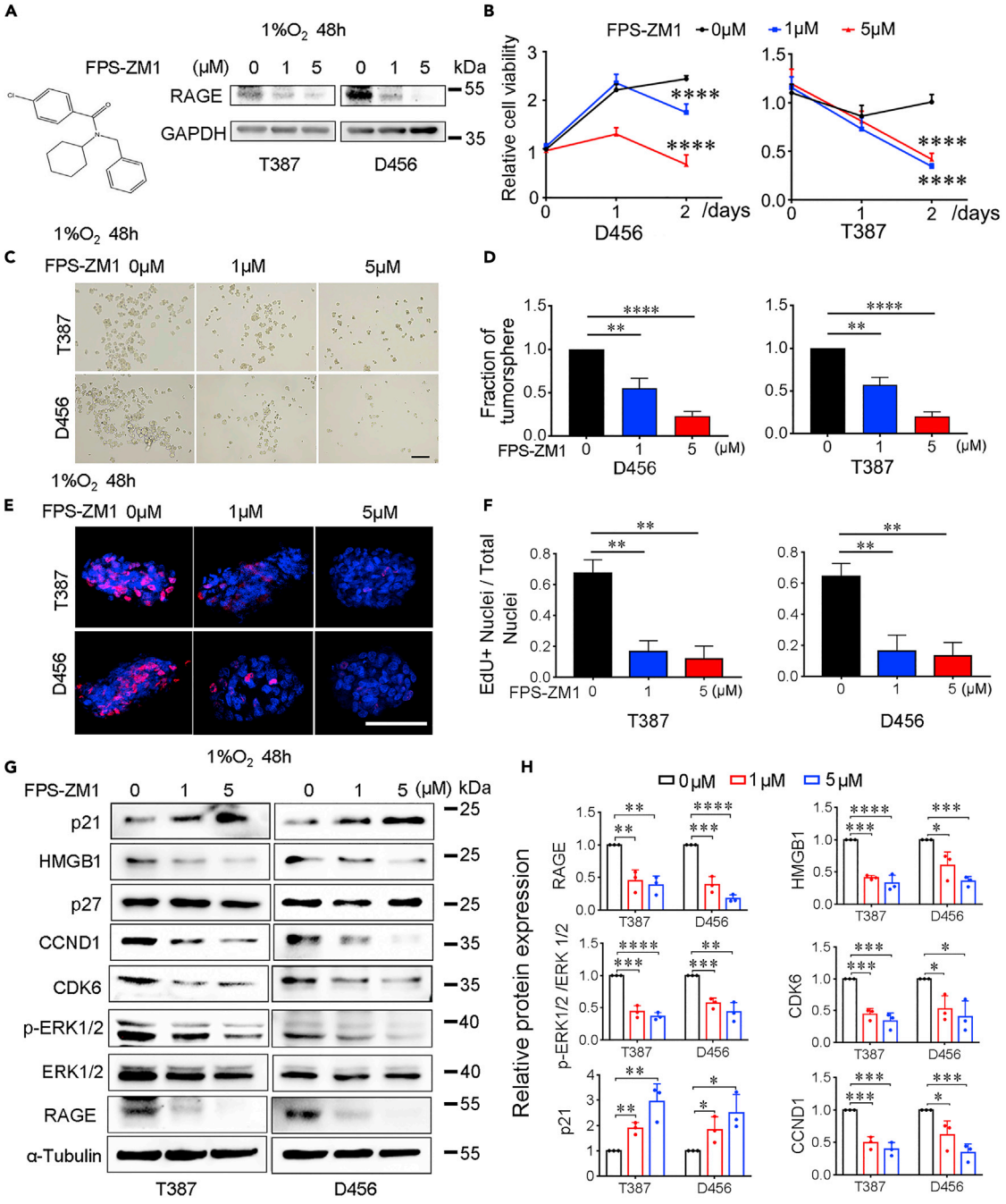

Figure 6. Inhibition of RAGE impairs the self-renewal of GSCs

(A) The chemical structure of FPS-ZM1 and Western blot analysis of RAGE expression in GSCs after FPS-ZM1 treatment for 48 h under hypoxia.

(B) Cell viability of GSCs treated with FPS-ZM1 under hypoxia. 0 μm FPS-ZM1 (DMSO treatment) served as control group. Data are normalized to day 0 group and represented as mean ± SD Significance was determined by two-tailed unpaired Student's *t* test. n = 3 replicates for each group. ****, $p < 0.0001$, compared to 0 μm group.

(C and D) Tumorsphere formation analysis of GSCs treated with FPS-ZM1 under hypoxia for 48 h. (C) Representative images are shown. Scale bar, 50 μm. (D) Quantitative analysis of tumorshpere number. Data are normalized to 0 μm group and represented as mean ± SD Significance was tested by two-tailed unpaired Student's *t* test. n = 3 replicates for each group. **, $p < 0.01$; ****, $p < 0.0001$.

(E and F) Fluorescent images and quantitative analysis of EdU incorporation in GSC tumorsphere under hypoxia for 48 h. (E) Representative images are shown. Scale bar, 50 μm. (F) Quantitative analysis of the fraction of EdU positive (+) cells. Data are represented as mean ± SD Significance was determined by two-tailed unpaired Student's *t* test. n = 3 replicates for each group. **, $p < 0.01$.

Figure 6. *Continued*
(G and H) Western blot and quantitative analysis of the expression of HMGB1 and RAGE-dependent ERK1/2 signaling molecules in GSCs treated with FPS-ZM1 for 48 h under hypoxia. (G) Representative blots are shown. (H) Data are normalized to 0 μM FPS-ZM1 (DMSO treatment) group and represented as mean ± SD Significance was determined by two-tailed unpaired Student's *t* test. n = 3 replicates for each group. *, $p < 0.05$; **, $p < 0.01$; ***, $p < 0.001$; ****, $p < 0.0001$.

Inhibition of RAGE attenuates the tumorigenic potential of GSCs

We further determined the role of RAGE-dependent ERK1/2 signaling pathway in regulating GSC growth. FPS-ZM1, a high-affinity and nontoxic RAGE-specific inhibitor (Fan et al., 2020; Shen et al., 2017), was used to inhibit the expression of RAGE in GSC lines (D456 and T387) (Figure 6A). We found that FPS-ZM1 significantly decreased the cell viability of GSCs (Figure 6B) and attenuated tumorsphere formation under hypoxia for 48 h (Figures 6C and 6D). EdU staining assay indicated that FPS-ZM1 inhibited proliferation of GSCs under hypoxia for 48 h (Figures 6E and 6F). Notably, FPS-ZM1 reduced the expression of both RAGE and HMGB1 in GSCs under hypoxic conditions. Correspondingly, both ERK1/2 phosphorylation levels and the expression of CCND1 and CDK6 were dramatically decreased, while p21 expression was increased in the groups treated with FPS-ZM1 (Figures 6G and 6H). FPS-ZM1 treatment showed no effect on p27 expression (Figure 6G). Together, these data indicate that FPS-ZM1 induces cell cycle arrest and inhibits cell renewal ability of GSCs subjected to hypoxia by disturbing RAGE-dependent ERK1/2 signaling pathway.

DISCUSSION

GBM is a very lethal brain tumor with a 16–18 months median survival interval from initial diagnosis (Ostrom et al., 2020). Therefore, the development of novel targets for therapeutic approaches to GBM is most needed. In the present study, we document that HMGB1 expression is elevated in patients with higher grade glioma, which is consistent with previous reports (Cheng et al., 2018; Wang et al., 2015). HMGB1 is highly expressed in stem-like cells in the human GBM specimens. More HMGB1-positive cells were observed in hypoxic regions of GBM. Hypoxia is a key microenvironment to maintain GSCs via activating HIF-1α and HIF-1α-dependent genes (Papale et al., 2020). We found that the levels of HIF-1α and HMGB1 are elevated in D456 and T387 GSCs subjected to hypoxia for 24 h. However, after exposure to hypoxia for 48 h, GSCs display a decline in the expression of HIF-1α and HMGB1. It has been reported that HIF-1α levels decrease in cells during prolonged exposure to hypoxia (Wiesener et al., 1998; Marxsen et al., 2004). Hypoxia induces the accumulation of prolylhydroxylase to promote proteasomal degradation of HIF-1α, leading to limited steady-state levels of HIF-1α under hypoxic conditions (Marxsen et al., 2004). In our work, DMOG upregulates both HIF-1α and HMGB1 in GSCs under normoxic conditions. In contrast, silencing HIF-1α dramatically inhibits the expression of HMGB1 in GSCs under hypoxia. These results indicate that HIF-1α is involved in regulating HMGB1 expression in GSCs subjected to hypoxia. Hypoxia is the distinct feature of niches where GSCs reside and are maintained (Aderetti et al., 2018). A variety of signaling pathways are involved in regulating the self-renewal and stemness maintenance of GSCs (Song et al., 2021). Here, our findings indicate that HMGB1 helps initiate GSCs stemness under early hypoxic stress.

Accompanying with activation of HIF under hypoxia, DAMPs or alarmins are released from various types of cells including tumor cells into extracellular space (Hernandez et al., 2016). These cytokines compose important components in the microenvironment and promote tumor cells proliferation and survival (Afshar-Sterle et al., 2014). Here, we identified that HIF-1α-positive tumor cells show an increased ratio of cytoplasmic to nuclear HMGB1 in human GBM specimens. Patients with GBM display high serum HMGB1 levels. Hypoxia promotes HMGB1 release from GSC lines *in vitro*. HMGB1 was initially discovered as a nuclear chromatin-binding protein (Bianchi et al., 1989), which was involved in the maintenance of nuclear homeostasis (Travers, 2003). HMGB1 is translocated from the nucleus into the cytoplasm via post-translational modifications including acetylation, phosphorylation, and methylation (Xue et al., 2021). Accumulating evidence indicates that tumor cells actively secrete or passively release HMGB1 to promote tumor regrowth, proliferation, and metastasis (Luo et al., 2013; Huang et al., 2018; van Beijnum et al., 2012). Active secretion of HMGB1 occurs via exocytosis of secretory lysosomes or exosomes (Murao et al., 2021). Hypoxia can induce living tumor cells to actively secrete HMGB1 in several types of tumor (Cheng et al., 2018; Tsung et al., 2007; Tang et al., 2010b; Yan et al., 2012). In our work, GSCs with shNT display increased cell number in hypoxia for 5 days, indicating these cells keep active proliferation. Thereby, GSCs might actively secrete HMGB1 into the extracellular matrix under hypoxia.

Notably, tumor cells would sense alarmins in hypoxic microenvironment through membrane receptors, triggering the activation of signaling pathways to uphold cell proliferation and tumor invasion (Papale

et al., 2020; Patel, 2018). RAGE is the major receptor responsible for HMGB1-mediated tumor cells growth (Kang et al., 2014a). In some solid tumors including colorectal cancer, the interaction of HMGB1 and RAGE is related to tumor growth and poor patient survival (Ellerman et al., 2007; Zhao et al., 2014). The promoter region of the RAGE gene contains HRE (Loboda et al., 2010). HIF-1α upregulates RAGE expression by recognizing HRE under hypoxia (Pichiule et al., 2007). Increased expression of RAGE has been reported in several ischemic hypoxia models (Zhai et al., 2008; Zeng et al., 2009). In the present study, we document that hypoxia dramatically augments the levels of RAGE mRNA in GSCs. HMGB1 knockdown significantly reduced RAGE expression, indicating that RAGE is key for HMGB1 regulating GSC proliferation. Additionally, FPS-ZM1, a small molecule that can suppress RAGE expression (Wang et al., 2018), downregulated the levels of RAGE and HMGB1 in GSCs under hypoxia. Similar with HMGB1 knockdown, FPS-ZM1 significantly weakened cell viability and tumorsphere formation ability of GSCs subjected to hypoxia. Collectively, hypoxia-induced HMGB1 is implicated in regulating the survival and self-renewal of GSCs via RAGE.

The engagement of RAGE and its ligands triggers signaling pathway cascade including ERK, PI3K/AKT, and Jak/STAT pathways (Oh et al., 2018; Kang et al., 2014b; Taneja et al., 2021). ERK binds intracellularly to the cytoplasmic domain of RAGE (Ishihara et al., 2003), integrating external signals into signaling events promoting cell growth and proliferation in many cell types including glioma cells (Huang et al., 2018; Tang et al., 2021; Wang et al., 2019). Furthermore, ERK1/2 phosphorylation causes a cascade activation of signaling molecules related to cell cycle, contributing to excessive tumor cell proliferation (Ebisuya et al., 2005; Marshall, 1995; Dent, 2013). In this study, the silence of HMGB1 inhibits the phosphorylation of ERK1/2 and reduces the expression of cell cycle molecules, which finally impairs the proliferation of GSCs both *in vitro* and *in vivo*. Moreover, shHMGB1 xenograft mice display longer survival than shNT mice, indicating that HMGB1 may serve as a therapeutic target in GBM.

Extracellular HMGB1 is released from necrotic, immune, and tumor cells, which in turn promotes the survival of tumor cells (Qin et al., 2014; Hoste et al., 2015; Jia et al., 2014; Zhang et al., 2019b). It has been reported that necrotic human T98G glioblastoma cells release HMGB1 upon death. Extracellular HMGB1 promotes the proliferative properties of T98G glioblastoma cells (Bassi et al., 2008). In addition, HMGB1 is also released from U118 glioblastoma cells under hypoxic conditions, stimulating cell proliferation and invasion (Cheng et al., 2018). In conclusion, extracellular HMGB1 in the hypoxia microenvironment may be derived from different subsets of tumor cells or immune cells in GBM. HMGB1 in the tumor microenvironment can serve as an autocrine and/or paracrine factor to guide cell cycle progression and regulate GSCs self-renewal via RAGE-dependent ERK1/2 signaling pathway, further facilitating tumor progression and recurrence. Thereby, targeting HMGB1 may be a potential therapeutic strategy for GBM.

Limitations of the study

We reveal that HIF-1α is associated with the elevation of HMGB1 expression in GSCs under hypoxic conditions. However, how HIF-1α regulates the expression of HMGB1 under hypoxia is unclear. The mechanism of HMGB1 release from GSCs subjected to hypoxia is also unclear. Further studies could be considered to extend the present work in the future.

STAR★METHODS

Detailed methods are provided in the online version of this paper and include the following:

- KEY RESOURCES TABLE
- RESOURCE AVAILABILITY
  - Lead contact
  - Materials availability
  - Data and code availability
- EXPERIMENTAL MODEL AND SUBJECT DETAILS
  - Human studies
  - Mouse xenografts
  - Cell lines
- METHOD DETAILS
  - shRNA plasmids and lentiviral transfection
  - Immunohistochemistry (IHC) and immunofluorescent (IF) staining
  - RNA isolation and quantitative real-time PCR (qPCR)

- Western blot analysis
- Cell viability assays
- 5-ethynyl-20-deoxyuridine (EdU) incorporation assay
- Tumorsphere formation assay and *in vitro* limiting dilution assay
- ELISA assay
- Bioinformatics analysis

● QUANTIFICATION AND STATISTICAL ANALYSIS

SUPPLEMENTAL INFORMATION

Supplemental information can be found online at https://doi.org/10.1016/j.isci.2022.104872.

ACKNOWLEDGMENTS

We thank Dr. Jeremy N Rich (Department of Neurology, University of Pittsburgh, Pittsburgh, Pennsylvania) and Dr. Shideng Bao (Department of Cancer Biology, Lerner Research Institute, Cleveland Clinic, Cleveland, USA) for providing GSC lines. Funding: This work was supported by Program for HUST Academic Frontier Youth Team, Huazhong University of Science and Technology Independent Innovation Research Fund Project (2019kfyXJJS187), and National Natural Science Foundation of China (81974452).

AUTHOR CONTRIBUTIONS

C.F.Y. and H.L. performed experiments and analyzed data. Y.Z., H.L.M., and Y.C.L. assisted with part of experiments *in vitro* and *in vivo*. G.H.L. performed bioinformatics analysis. X.J.Y. and Q.G.X. obtained ethical approval and supervised human sample collection. H.L.L. and L.N. performed pathological analysis. X.J.Y. and C.F.Y. conceived the study. C.F.Y. wrote the manuscript with contribution from all authors.

DECLARATION OF INTERESTS

The authors declare no competing interests.

Received: February 7, 2022
Revised: June 10, 2022
Accepted: July 29, 2022
Published: September 16, 2022

REFERENCES

Aderetti, D.A., Hira, V.V.V., Molenaar, R.J., and van Noorden, C.J.F. (2018). The hypoxic peri-arteriolar glioma stem cell niche, an integrated concept of five types of niches in human glioblastoma. Biochim. Biophys. Acta. Rev. Cancer *1869*, 346–354. https://doi.org/10.1016/j.bbcan.2018.04.008.

Afshar-Sterle, S., Zotos, D., Bernard, N.J., Scherger, A.K., Rödling, L., Alsop, A.E., Walker, J., Masson, F., Belz, G.T., Corcoran, L.M., et al. (2014). Fas ligand-mediated immune surveillance by T cells is essential for the control of spontaneous B cell lymphomas. Nat. Med. *20*, 283–290. https://doi.org/10.1038/nm.3442.

Bahrami, A., Hesari, A., Khazaei, M., Hassanian, S.M., Ferns, G.A., and Avan, A. (2018). The therapeutic potential of targeting the BRAF mutation in patients with colorectal cancer. J. Cell. Physiol. *233*, 2162–2169. https://doi.org/10.1002/jcp.25952.

Bao, L., Chen, Y., Lai, H.T., Wu, S.Y., Wang, J.E., Hatanpaa, K.J., Raisanen, J.M., Fontenot, M., Lega, B., Chiang, C.M., et al. (2018). Methylation of hypoxia-inducible factor (HIF)-1α by G9a/GLP inhibits HIF-1 transcriptional activity and cell migration. Nucleic Acids Res. *46*, 6576–6591. https://doi.org/10.1093/nar/gky449.

Bassi, R., Giussani, P., Anelli, V., Colleoni, T., Pedrazzi, M., Patrone, M., Viani, P., Sparatore, B., Melloni, E., and Riboni, L. (2008). HMGB1 as an autocrine stimulus in human T98G glioblastoma cells: role in cell growth and migration. J. Neuro Oncol. *87*, 23–33. https://doi.org/10.1007/s11060-007-9488-y.

Bianchi, M.E., Beltrame, M., and Paonessa, G. (1989). Specific recognition of cruciform DNA by nuclear protein HMG1. Science *243*, 1056–1059. https://doi.org/10.1126/science.2922595.

Bianchi, M.E. (2007). DAMPs, PAMPs and alarmins: all we need to know about danger. J. Leukoc. Biol. *81*, 1–5. https://doi.org/10.1189/jlb.0306164.

Cheng, P., Ma, Y., Gao, Z., and Duan, L. (2018). High mobility group box 1 (HMGB1) predicts invasion and poor prognosis of glioblastoma multiforme via activating AKT signaling in an autocrine pathway. Med. Sci. Monit. *24*, 8916–8924. https://doi.org/10.12659/MSM.912104.

Colwell, N., Larion, M., Giles, A.J., Seldomridge, A.N., Sizdahkhani, S., Gilbert, M.R., and Park, D.M. (2017). Hypoxia in the glioblastoma microenvironment: shaping the phenotype of cancer stem-like cells. Neuro Oncol. *19*, 887–896. https://doi.org/10.1093/neuonc/now258.

Crozier, L., Foy, R., Mouery, B.L., Whitaker, R.H., Corno, A., Spanos, C., Ly, T., Gowen Cook, J., and Saurin, A.T. (2022). CDK4/6 inhibitors induce replication stress to cause long-term cell cycle withdrawal. EMBO J. *41*, e108599. https://doi.org/10.15252/embj.2021108599.

Dent, P. (2013). ERK plays the baddie (again). Cancer Biol. Ther. *14*, 997–998. https://doi.org/10.4161/cbt.26377.

Dumas, A.A., Pomella, N., Rosser, G., Guglielmi, L., Vinel, C., Millner, T.O., Rees, J., Aley, N., Sheer, D., Wei, J., et al. (2020). Microglia promote glioblastoma via mTOR-mediated immunosuppression of the tumour microenvironment. EMBO J. *39*, e103790. https://doi.org/10.15252/embj.2019103790.

Ebisuya, M., Kondoh, K., and Nishida, E. (2005). The duration, magnitude and compartmentalization of ERK MAP kinase activity: mechanisms for providing signaling specificity. J. Cell Sci. *118*, 2997–3002. https://doi.org/10.1242/jcs.02505.

Eckel-Passow, J.E., Lachance, D.H., Molinaro, A.M., Walsh, K.M., Decker, P.A., Sicotte, H., Pekmezci, M., Rice, T., Kosel, M.L., Smirnov, I.V., et al. (2015). Glioma groups based on 1p/19q, IDH, and TERT promoter mutations in tumors. N. Engl. J. Med. *372*, 2499–2508. https://doi.org/10.1056/NEJMoa1407279.

Ellerman, J.E., Brown, C.K., de Vera, M., Zeh, H.J., Billiar, T., Rubartelli, A., and Lotze, M.T. (2007). Masquerader: high mobility group box-1 and cancer. Clin. Cancer Res. *13*, 2836–2848. https://doi.org/10.1158/1078-0432.CCR-06-1953.

Fan, H., Tang, H.B., Chen, Z., Wang, H.Q., Zhang, L., Jiang, Y., Li, T., Yang, C.F., Wang, X.Y., Li, X., et al. (2020). Inhibiting HMGB1-RAGE axis prevents pro-inflammatory macrophages/microglia polarization and affords neuroprotection after spinal cord injury. J. Neuroinflammation *17*, 295. https://doi.org/10.1186/s12974-020-01973-4.

Gabriely, G., Wheeler, M.A., Takenaka, M.C., and Quintana, F.J. (2017). Role of AHR and HIF-1α in glioblastoma metabolism. Trends Endocrinol. Metab. *28*, 428–436. https://doi.org/10.1016/j.tem.2017.02.009.

Gao, X.Y., Zang, J., Zheng, M.H., Zhang, Y.F., Yue, K.Y., Cao, X.L., Cao, Y., Li, X.X., Han, H., Jiang, X.F., et al. (2021). Temozolomide treatment induces HMGB1 to promote the formation of glioma stem cells via the TLR2/NEAT1/Wnt pathway in glioblastoma. Front. Cell Dev. Biol. *9*, 620883. https://doi.org/10.3389/fcell.2021.620883.

Gimple, R.C., Bhargava, S., Dixit, D., and Rich, J.N. (2019). Glioblastoma stem cells: lessons from the tumor hierarchy in a lethal cancer. Genes Dev. *33*, 591–609. https://doi.org/10.1101/gad.324301.119.

Hambardzumyan, D., and Bergers, G. (2015). Glioblastoma: defining tumor niches. Trends Cancer *1*, 252–265. https://doi.org/10.1016/j.trecan.2015.10.009.

Heddleston, J.M., Li, Z., McLendon, R.E., Hjelmeland, A.B., and Rich, J.N. (2009). The hypoxic microenvironment maintains glioblastoma stem cells and promotes reprogramming towards a cancer stem cell phenotype. Cell Cycle *8*, 3274–3284. https://doi.org/10.4161/cc.8.20.9701.

Hernandez, C., Huebener, P., and Schwabe, R.F. (2016). Damage-associated molecular patterns in cancer: a double-edged sword. Oncogene *35*, 5931–5941. https://doi.org/10.1038/onc.2016.104.

He, S., Cheng, J., Sun, L., Wang, Y., Wang, C., Liu, X., Zhang, Z., Zhao, M., Luo, Y., Tian, L., et al. (2018). HMGB1 released by irradiated tumor cells promotes living tumor cell proliferation via paracrine effect. Cell Death Dis. *9*, 648. https://doi.org/10.1038/s41419-018-0626-6.

Hoste, E., Arwert, E.N., Lal, R., South, A.P., Salas-Alanis, J.C., Murrell, D.F., Donati, G., and Watt, F.M. (2015). Innate sensing of microbial products promotes wound-induced skin cancer. Nat. Commun. *6*, 5932. https://doi.org/10.1038/ncomms6932.

Hu, Y., and Smyth, G.K. (2009). ELDA: extreme limiting dilution analysis for comparing depleted and enriched populations in stem cell and other assays. J. Immunol. Methods *347*, 70–78. https://doi.org/10.1016/j.jim.2009.06.008.

Huang, C.Y., Chiang, S.F., Chen, W.T.L., Ke, T.W., Chen, T.W., You, Y.S., Lin, C.Y., Chao, K.S.C., and Huang, C.Y. (2018). HMGB1 promotes ERK-mediated mitochondrial Drp1 phosphorylation for chemoresistance through RAGE in colorectal cancer. Cell Death Dis. *9*, 1004. https://doi.org/10.1038/s41419-018-1019-6.

Huang, H., Yu, X., Han, X., Hao, J., Zhao, J., Bebek, G., Bao, S., Prayson, R.A., Khalil, A.M., Jankowsky, E., et al. (2021). Piwil1 regulates glioma stem cell maintenance and glioblastoma progression. Cell Rep. *34*, 108522. https://doi.org/10.1016/j.celrep.2020.108522.

Huang, S., Qi, P., Zhang, T., Li, F., and He, X. (2019). The HIF-1α/miR-224-3p/ATG5 axis affects cell mobility and chemosensitivity by regulating hypoxia-induced protective autophagy in glioblastoma and astrocytoma. Oncol. Rep. *41*, 1759–1768. https://doi.org/10.3892/or.2018.6929.

Ishihara, K., Tsutsumi, K., Kawane, S., Nakajima, M., and Kasaoka, T. (2003). The receptor for advanced glycation end-products (RAGE) directly binds to ERK by a D-domain-like docking site. FEBS Lett. *550*, 107–113. https://doi.org/10.1016/s0014-5793(03)00846-9.

Jia, L., Clear, A., Liu, F.T., Matthews, J., Uddin, N., McCarthy, A., Hoxha, E., Durance, C., Iqbal, S., and Gribben, J.G. (2014). Extracellular HMGB1 promotes differentiation of nurse-like cells in chronic lymphocytic leukemia. Blood *123*, 1709–1719. https://doi.org/10.1182/blood-2013-10-529610.

Jube, S., Rivera, Z.S., Bianchi, M.E., Powers, A., Wang, E., Pagano, I., Pass, H.I., Gaudino, G., Carbone, M., and Yang, H. (2012). Cancer cell secretion of the DAMP protein HMGB1 supports progression in malignant mesothelioma. Cancer Res. *72*, 3290–3301. https://doi.org/10.1158/0008-5472.CAN-11-3481.

Kang, R., Tang, D., Schapiro, N.E., Loux, T., Livesey, K.M., Billiar, T.R., Wang, H., Van Houten, B., Lotze, M.T., and Zeh, H.J. (2014a). The HMGB1/RAGE inflammatory pathway promotes pancreatic tumor growth by regulating mitochondrial bioenergetics. Oncogene *33*, 567–577. https://doi.org/10.1038/onc.2012.631.

Kang, R., Hou, W., Zhang, Q., Chen, R., Lee, Y.J., Bartlett, D.L., Lotze, M.T., Tang, D., and Zeh, H.J. (2014b). RAGE is essential for oncogenic KRAS-mediated hypoxic signaling in pancreatic cancer. Cell Death Dis. *5*, e1480. https://doi.org/10.1038/cddis.2014.445.

Li, S., Wang, J., Wei, Y., Liu, Y., Ding, X., Dong, B., Xu, Y., and Wang, Y. (2015). Crucial role of TRPC6 in maintaining the stability of HIF-1α in glioma cells under hypoxia. J. Cell Sci. *128*, 3317–3329. https://doi.org/10.1242/jcs.173161.

Li, Z., Bao, S., Wu, Q., Wang, H., Eyler, C., Sathornsumetee, S., Shi, Q., Cao, Y., Lathia, J., McLendon, R.E., et al. (2009). Hypoxia-inducible factors regulate tumorigenic capacity of glioma stem cells. Cancer Cell *15*, 501–513. https://doi.org/10.1016/j.ccr.2009.03.018.

Loboda, A., Jozkowicz, A., and Dulak, J. (2010). HIF-1 and HIF-2 transcription factors–similar but not identical. Mol. Cells *29*, 435–442. https://doi.org/10.1007/s10059-010-0067-2.

Luo, Y., Chihara, Y., Fujimoto, K., Sasahira, T., Kuwada, M., Fujiwara, R., Fujii, K., Ohmori, H., and Kuniyasu, H. (2013). High mobility group box 1 released from necrotic cells enhances regrowth and metastasis of cancer cells that have survived chemotherapy. Eur. J. Cancer *49*, 741–751. https://doi.org/10.1016/j.ejca.2012.09.016.

Man, J., Yu, X., Huang, H., Zhou, W., Xiang, C., Huang, H., Miele, L., Liu, Z., Bebek, G., Bao, S., et al. (2018). Hypoxic induction of vasorin regulates Notch1 turnover to maintain glioma stem-like cells. Cell Stem Cell *22*, 104–118.e6. https://doi.org/10.1016/j.stem.2017.10.005.

Man, J., Shoemake, J., Zhou, W., Fang, X., Wu, Q., Rizzo, A., Prayson, R., Bao, S., Rich, J.N., and Yu, J.S. (2014). Sema3C promotes the survival and tumorigenicity of glioma stem cells through Rac1 activation. Cell Rep. *9*, 1812–1826. https://doi.org/10.1016/j.celrep.2014.10.055.

Marshall, C.J. (1995). Specificity of receptor tyrosine kinase signaling: transient versus sustained extracellular signal-regulated kinase activation. Cell *80*, 179–185. https://doi.org/10.1016/0092-8674(95)90401-8.

Marxsen, J.H., Stengel, P., Doege, K., Heikkinen, P., Jokilehto, T., Wagner, T., Jelkmann, W., Jaakkola, P., and Metzen, E. (2004). Hypoxia-inducible factor-1 (HIF-1) promotes its degradation by induction of HIF-alpha-prolyl-4-hydroxylases. Biochem. J. *381*, 761–767. https://doi.org/10.1042/BJ20040620.

Murao, A., Aziz, M., Wang, H., Brenner, M., and Wang, P. (2021). Release mechanisms of major DAMPs. Apoptosis *26*, 152–162. https://doi.org/10.1007/s10495-021-01663-3.

Oh, H.N., Seo, J.H., Lee, M.H., Yoon, G., Cho, S.S., Liu, K., Choi, H., Oh, K.B., Cho, Y.S., Kim, H., et al. (2018). Oridonin induces apoptosis in oral squamous cell carcinoma probably through the generation of reactive oxygen species and the p38/JNK MAPK pathway. Int. J. Oncol. *52*, 1749–1759. https://doi.org/10.3892/ijo.2018.4319.

Ostrom, Q.T., Patil, N., Cioffi, G., Waite, K., Kruchko, C., and Barnholtz-Sloan, J.S. (2020). CBTRUS statistical report: primary brain and other central nervous system tumors diagnosed in the United States in 2013-2017. Neuro Oncol. *22*, iv1–iv96. https://doi.org/10.1093/neuonc/noaa200.

Papale, M., Buccarelli, M., Mollinari, C., Russo, M.A., Pallini, R., Ricci-Vitiani, L., and Tafani, M. (2020). Hypoxia, inflammation and necrosis as determinants of glioblastoma cancer stem cells progression. Int. J. Mol. Sci. *21*, 2660. https://doi.org/10.3390/ijms21082660.

Patel, S. (2018). Danger-associated molecular patterns (DAMPs): the derivatives and triggers of inflammation. Curr. Allergy Asthma Rep. *18*, 63. https://doi.org/10.1007/s11882-018-0817-3.

Pichiule, P., Chavez, J.C., Schmidt, A.M., and Vannucci, S.J. (2007). Hypoxia-inducible factor-1 mediates neuronal expression of the receptor for advanced glycation end products following hypoxia/ischemia. J. Biol. Chem. *282*, 36330–36340. https://doi.org/10.1074/jbc.M706407200.

Qian, F., Xiao, J., Gai, L., and Zhu, J. (2019). HMGB1-RAGE signaling facilitates Ras-dependent Yap1 expression to drive colorectal cancer stemness and development. Mol. Carcinog. *58*, 500–510. https://doi.org/10.1002/mc.22944.

Qin, Y., Chen, Y., Wang, W., Wang, Z., Tang, G., Zhang, P., He, Z., Liu, Y., Dai, S.M., and Shen, Q. (2014). HMGB1-LPS complex promotes transformation of osteoarthritis synovial fibroblasts to a rheumatoid arthritis synovial fibroblast-like phenotype. Cell Death Dis. *5*, e1077. https://doi.org/10.1038/cddis.2014.48.

Rapoport, B.L., Steel, H.C., Theron, A.J., Heyman, L., Smit, T., Ramdas, Y., and Anderson, R. (2020). High mobility group box 1 in human cancer. Cells *9*, 1664. https://doi.org/10.3390/cells9071664.

Rider, P., Kaplanov, I., Romzova, M., Bernardis, L., Braiman, A., Voronov, E., and Apte, R.N. (2012). The transcription of the alarmin cytokine interleukin-1 alpha is controlled by hypoxia inducible factors 1 and 2 alpha in hypoxic cells. Front. Immunol. *3*, 290. https://doi.org/10.3389/fimmu.2012.00290.

Rong, Y., Durden, D.L., Van Meir, E.G., and Brat, D.J. (2006). Pseudopalisading' necrosis in glioblastoma: a familiar morphologic feature that links vascular pathology, hypoxia, and angiogenesis. J. Neuropathol. Exp. Neuro. *65*, 529–539. https://doi.org/10.1097/00005072-200606000-00001.

Russo, M.A., Sansone, L., Carnevale, I., Limana, F., Runci, A., Polletta, L., Perrone, G.A., De Santis, E., and Tafani, M. (2015). One special question to start with: can HIF/NFkB be a target in inflammation? Endocr. Metab. Immune Disord. Drug Targets *15*, 171–185. https://doi.org/10.2174/1871530315666150316120112.

Schneider, C.A., Rasband, W.S., and Eliceiri, K.W. (2012). NIH Image to ImageJ: 25 years of image analysis. Nat. Methods *9*, 671–675. https://doi.org/10.1038/nmeth.2089.

Seidel, S., Garvalov, B.K., Wirta, V., von Stechow, L., Schänzer, A., Meletis, K., Wolter, M., Sommerlad, D., Henze, A.T., Nistér, M., et al. (2010). A hypoxic niche regulates glioblastoma stem cells through hypoxia inducible factor 2 alpha. Brain *133* (Pt 4), 983–995. https://doi.org/10.1093/brain/awq042.

Shen, C., Ma, Y., Zeng, Z., Yin, Q., Hong, Y., Hou, X., and Liu, X. (2017). RAGE-specific inhibitor FPS-ZM1 attenuates AGEs-induced neuroinflammation and oxidative stress in rat primary microglia. Neurochem. Res. *42*, 2902–2911. https://doi.org/10.1007/s11064-017-2321-x.

Soeda, A., Park, M., Lee, D., Mintz, A., Androutsellis-Theotokis, A., McKay, R.D., Engh, J., Iwama, T., Kunisada, T., Kassam, A.B., et al. (2009). Hypoxia promotes expansion of the CD133-positive glioma stem cells through activation of HIF-1alpha. Oncogene *28*, 3949–3959. https://doi.org/10.1038/onc.2009.252.

Song, S., Ma, D., Xu, L., Wang, Q., Liu, L., Tong, X., and Yan, H. (2021). Low-intensity pulsed ultrasound-generated singlet oxygen induces telomere damage leading to glioma stem cell awakening from quiescence. iScience *25*, 103558. https://doi.org/10.1016/j.isci.2021.103558.

Tafani, M., Di Vito, M., Frati, A., Pellegrini, L., De Santis, E., Sette, G., Eramo, A., Sale, P., Mari, E., Santoro, A., et al. (2011). Pro-inflammatory gene expression in solid glioblastoma microenvironment and in hypoxic stem cells from human glioblastoma. J. Neuroinflammation *8*, 32. https://doi.org/10.1186/1742-2094-8-32.

Taneja, S., Vetter, S.W., and Leclerc, E. (2021). Hypoxia and the receptor for advanced glycation end products (RAGE) signaling in cancer. Int. J. Mol. Sci. *22*, 8153. https://doi.org/10.3390/ijms22158153.

Tang, D., Kang, R., Cheh, C.W., Livesey, K.M., and Lotze, M.T. (2010a). High-mobility group box 1 and cancer. Biochim. Biophys. Acta *1799*, 131–140. https://doi.org/10.1016/j.bbagrm.2009.11.014.

Tang, D., Kang, R., Cheh, C.W., Livesey, K.M., Liang, X., Schapiro, N.E., Benschop, R., Sparvero, L.J., Amoscato, A.A., Tracey, K.J., et al. (2010b). HMGB1 release and redox regulates autophagy and apoptosis in cancer cells. Oncogene *29*, 5299–5310. https://doi.org/10.1038/onc.2010.261.

Tang, T., Wang, S., Cai, T., Cheng, Z., Meng, Y., Qi, S., Zhang, Y., and Qi, Z. (2021). High mobility group box 1 regulates gastric cancer cell proliferation and migration via RAGE-mTOR/ERK feedback loop. J. Cancer *12*, 518–529. https://doi.org/10.7150/jca.51049.

Travers, A.A. (2003). Priming the nucleosome: a role for HMGB proteins? EMBO Rep. *4*, 131–136. https://doi.org/10.1038/sj.embor.embor741.

Tsung, A., Klune, J.R., Zhang, X., Jeyabalan, G., Cao, Z., Peng, X., Stolz, D.B., Geller, D.A., Rosengart, M.R., and Billiar, T.R. (2007). HMGB1 release induced by liver ischemia involves Toll-like receptor 4 dependent reactive oxygen species production and calcium-mediated signaling. J. Exp. Med. *204*, 2913–2923. https://doi.org/10.1084/jem.20070247.

van Beijnum, J.R., Nowak-Sliwinska, P., van den Boezem, E., Hautvast, P., Buurman, W.A., and Griffioen, A.W. (2012). Tumor angiogenesis is enforced by autocrine regulation of high-mobility group box 1. Oncogene *32*, 363–374. https://doi.org/10.1038/onc.2012.49.

Wang, H., Chen, F., Du, Y.F., Long, Y., Reed, M.N., Hu, M., Suppiramaniam, V., Hong, H., and Tang, S.S. (2018). Targeted inhibition of RAGE reduces amyloid-β influx across the blood-brain barrier and improves cognitive deficits in db/db mice. Neuropharmacology *131*, 143–153. https://doi.org/10.1016/j.neuropharm.2017.12.026.

Wang, C., Zhao, N., Zheng, Q., Zhang, D., and Liu, Y. (2019). BHLHE41 promotes U87 and U251 cell proliferation via ERK/cyclinD1 signaling pathway. Cancer Manag. Res. *11*, 7657–7672. https://doi.org/10.2147/CMAR.S214697.

Wang, S., and Zhang, Y. (2020). HMGB1 in inflammation and cancer. J. Hematol. Oncol. *13*, 116. https://doi.org/10.1186/s13045-020-00950-x.

Wang, X.J., Zhou, S.L., Fu, X.D., Zhang, Y.Y., Liang, B., Shou, J.X., Wang, J.Y., and Ma, J. (2015). Clinical and prognostic significance of high-mobility group box-1 in human gliomas. Exp. Ther. Med. *9*, 513–518. https://doi.org/10.3892/etm.2014.2089.

Wakimoto, R., Ono, M., Takeshima, M., Higuchi, T., and Nakano, S. (2017). Differential anticancer activity of pterostilbene against three subtypes of human breast cancer cells. Anticancer Res. *37*, 6153–6159. https://doi.org/10.21873/anticanres.12064.

Wiesener, M.S., Turley, H., Allen, W.E., Willam, C., Eckardt, K.U., Talks, K.L., Wood, S.M., Gatter, K.C., Harris, A.L., Pugh, C.W., et al. (1998). Induction of endothelial PAS domain protein-1 by hypoxia: characterization and comparison with hypoxia-inducible factor-1α. Blood *92*, 2260–2268.

Wu, L., and Yang, L. (2018). The function and mechanism of HMGB1 in lung cancer and its potential therapeutic implications. Oncol. Lett. *15*, 6799–6805. https://doi.org/10.3892/ol.2018.8215.

Xu, P., Chen, C., Zhang, Y., Dzieciatkowska, M., Brown, B.C., Zhang, W., Xie, T., Abdulmalik, O., Song, A., Tong, C., et al. (2022). Erythrocyte transglutaminase-2 combats hypoxia and chronic kidney disease by promoting oxygen delivery and carnitine homeostasis. Cell Metab. *34*, 299–316.e6. https://doi.org/10.1016/j.cmet.2021.12.019.

Xue, J., Suarez, J.S., Minaai, M., Li, S., Gaudino, G., Pass, H.I., Carbone, M., and Yang, H. (2021). HMGB1 as a therapeutic target in disease. J. Cell. Physiol. *236*, 3406–3419. https://doi.org/10.1002/jcp.30125.

Yan, W., Chang, Y., Liang, X., Cardinal, J.S., Huang, H., Thorne, S.H., Monga, S.P.S., Geller, D.A., Lotze, M.T., and Tsung, A. (2012). High-mobility group box 1 activates caspase-1 and promotes hepatocellular carcinoma invasiveness and metastases. Hepatology *55*, 1863–1875. https://doi.org/10.1002/hep.25572.

Zeng, S., Dun, H., Ippagunta, N., Rosario, R., Zhang, Q.Y., Lefkowitch, J., Yan, S.F., Schmidt, A.M., and Emond, J.C. (2009). Receptor for advanced glycation end product (RAGE)-dependent modulation of early growth response-1 in hepatic ischemia/reperfusion injury. J. Hepatol. *50*, 929–936. https://doi.org/10.1016/j.jhep.2008.11.022.

Zhai, D.X., Kong, Q.F., Xu, W.S., Bai, S.S., Peng, H.S., Zhao, K., Li, G.Z., Wang, D.D., Sun, B., Wang, J.H., et al. (2008). RAGE expression is up-regulated in human cerebral ischemia and pMCAO rats. Neurosci. Lett. *445*, 117–121. https://doi.org/10.1016/j.neulet.2008.08.077.

Zhang, B., Chen, Y., Shi, X., Zhou, M., Bao, L., Hatanpaa, K.J., Patel, T., DeBerardinis, R.J., Wang, Y., and Luo, W. (2021). Regulation of branched-chain amino acid metabolism by hypoxia-inducible factor in glioblastoma. Cell. Mol. Life Sci. *78*, 195–206. https://doi.org/10.1007/s00018-020-03483-1.

Zhang, I.Y., Zhou, H., Liu, H., Zhang, L., Gao, H., Liu, S., Song, Y., Alizadeh, D., Yin, H.H., Pillai, R., et al. (2020). Local and systemic immune dysregulation alters glioma growth in hyperglycemic mice. Clin. Cancer Res. *26*, 2740–2753. https://doi.org/10.1158/1078-0432.CCR-19-2520.

Zhang, J., Shao, S., Han, D., Xu, Y., Jiao, D., Wu, J., Yang, F., Ge, Y., Shi, S., Li, Y., et al. (2018). High

mobility group box 1 promotes the epithelial-to-mesenchymal transition in prostate cancer PC3 cells via the RAGE/NF-κB signaling pathway. Int. J. Oncol. *53*, 659–671. https://doi.org/10.3892/ijo.2018.4420.

Zhang, L., Shi, H., Chen, H., Gong, A., Liu, Y., Song, L., Xu, X., You, T., Fan, X., Wang, D., et al. (2019a). Dedifferentiation process driven by radiotherapy-induced HMGB1/TLR2/YAP/HIF-1α signaling enhances pancreatic cancer stemness. Cell Death Dis. *10*, 724. https://doi.org/10.1038/s41419-019-1956-8.

Zhang, T., Guan, X.W., Gribben, J.G., Liu, F.T., and Jia, L. (2019b). Blockade of HMGB1 signaling pathway by ethyl pyruvate inhibits tumor growth in diffuse large B-cell lymphoma. Cell Death Dis. *10*, 330. https://doi.org/10.1038/s41419-019-1563-8.

Zhao, C.B., Bao, J.M., Lu, Y.J., Zhao, T., Zhou, X.H., Zheng, D.Y., and Zhao, S.C. (2014). Co-expression of RAGE and HMGB1 is associated with cancer progression and poor patient outcome of prostate cancer. Am. J. Cancer Res. *4*, 369–377.

Zhao, M., Zhang, Y., Jiang, Y., Wang, K., Wang, X., Zhou, D., Wang, Y., Yu, R., and Zhou, X. (2021). YAP promotes autophagy and progression of gliomas via upregulating HMGB1. J. Exp. Clin. Cancer Res. *40*, 99. https://doi.org/10.1186/s13046-021-01897-8.

Zhao, X.L., Lin, Y., Jiang, J., Tang, Z., Yang, S., Lu, L., Liang, Y., Liu, X., Tan, J., Hu, X.G., et al. (2017). High-mobility group box 1 released by autophagic cancer-associated fibroblasts maintains the stemness of luminal breast cancer cells. J. Pathol. *243*, 376–389. https://doi.org/10.1002/path.4958.

STAR★METHODS

KEY RESOURCES TABLE

REAGENT or RESOURCE	SOURCE	IDENTIFIER
Antibodies		
HMGB1 antibody	Affinity Biosciences	Cat#DF7008; RRID:AB_2838964
HMGB1 antibody	Santa Cruz Biotechnology	Cat#sc-74085; RRID:AB_1123993
Recombinant Anti-RAGE antibody	Abcam	Cat#ab216329; RRID:AB_2884897
Anti-SOX2 antibody	Abcam	Cat#ab171380; RRID:AB_2732072
Olig2 antibody	Proteintech	Cat#66513-1-Ig; RRID:AB_2881876
Anti-Olig2 monoclonal antibody	Millipore	Cat#MABN50; RRID:AB_10807410
GFAP (E4L7M) XP® Rabbit	Cell Signalling Technology	Cat#80788
Cleaved PARP (Asp214) (D64E10) XP Rabbit mAb antibody	Cell Signaling Technology	Cat#5625; RRID:AB_10699459
LaminB1 antibody	Proteintech	Cat #66095-1-Ig
Cyclin D1 Monoclonal antibody	Proteintech	Cat #60186-1-Ig
TLR2 (TL2.1) antibody	Santa Cruz Biotechnology	Cat#sc-21759; RRID:AB_628363
TLR4 (25) antibody	Santa Cruz Biotechnology	Cat#sc-21759; RRID:AB_10611320
p21 Waf1/Cip1 (12D1) Rabbit mAb antibody	Cell Signaling Technology	Cat#2947; RRID:AB_823586
GAPDH (0411) antibody	Santa Cruz Biotechnology	Cat#sc-47724; RRID:AB_627678
alpha Tubulin monoclonal antibody	ABclonal	Cat#AC012; RRID:AB_2768341
HIF-1 alpha antibody	Novus	Cat#NB100-449; RRID:AB_10001045
HIF1 alpha antibody	Abcam	Cat#ab51608; RRID:AB_880418
HIF1α antibody	Proteintech	Cat#66730-1-Ig; RRID:AB_2882080
HIF-2 alpha/EPAS1 antibody	Novus	Cat#NB100-122; RRID:AB_10002593
CDK4 antibody	Cell Signaling Technology	Cat#12790; RRID:AB_2631166
CDK6 (DCS83) mouse mAb antibody	Cell Signaling Technology	Cat#3136; RRID:AB_2229289
ERK1/2 antibody	Affinity Biosciences	Cat#AF0155; RRID:AB_2833336
Phospho-ERK1/2 (Thr202/Tyr204) antibody	Affinity Biosciences	Cat#AF1015; RRID:AB_2834432
CA9 (Carbonic Anhydrase IX) antibody	Novus	Cat#NB100-417; RRID:AB_10003398
CD15/SSEA1 (MC480) antibody	Cell Signaling Technology	Cat #4744
CD133 antibody	Affinity Biosciences	Cat#BF0403; RRID:AB_2833933
KI67 antibody	Proteintech	Cat#27309-1-AP; RRID:AB_2756525
Cleaved Caspase-3 (Asp175) (5A1E) rabbit mAb antibody	Cell Signaling Technology	Cat#9664; RRID:AB_2070042
Chemicals, peptides, and recombinant proteins		
FPS-ZM1	MedChemExpress	Cat#HY-19370
DMOG	Selleckchem	Cat#S7483
Matrigel	Absin	Cat#abs9410
Critical commercial assays		
2-stem plus Poly-HRP Anti-Mouse IgG Detection System	Beijing Zhongshan Jinqiao Biotechnology	Cat#PV-6002
2-stem plus Poly-HRP Anti-Rabbit IgG Detection System	Beijing Zhongshan Jinqiao Biotechnology	Cat#PV-6001
Reverse transcription kit HiScript II Q RT SuperMix	Vazyme	Cat#R223-01
ChamQ SYBR qPCR Master Mix	Vazyme	Cat#Q311-02/03
Cell Titer-Lumi™ Plus Luminescent Cell Viability Assay Kit	Beyotime	Cat#C0068S

(*Continued on next page*)

Continued

REAGENT or RESOURCE	SOURCE	IDENTIFIER
Human HMGB-1 ELISA kits	Jianglaibio	Cat#13693-96T
Cell-Light EdU Apollo-567 *In Vitro* Imaging Kit	RiboBio	Cat#C10310-1
Deposited data		
The clinical data of glioma patients and their corresponding gene expression profiles	TCGA or CGGA	http://gliovis.bioinfo.cnio.es/
Experimental models: Cell lines		
GSC T387	Gifts from Dr. Jeremy N Rich and Dr. Shideng Bao	N/A
GSC D456	Gifts from Dr. Jeremy N Rich and Dr. Shideng Bao	N/A
293T	ATCC	CRL-3216, RRID:CVCL_0063
Experimental models: Organisms/strains		
BALA/c Nude mice	Beijing Vital River Laboratory Animal Technology Co., Ltd	N/A
Oligonucleotides		
GAPDH primer: Forward 5′-GTCTCCTCTGACTTCAACAGCG-3′ Reverse 5′-ACCACCCTGTTGCTGTAGCCAA-3′	This paper	N/A
HMGB1 primer: Forward 5′-TATGGCAAAAGCGGACAAGG-3′ Reverse 5′-CTTCGCAACATCACCAATGGA-3′	This paper	N/A
HIF-1α primer: Forward 5′-AGTCTAGAGATGCAGCAAGATCTC-3′ Reverse 5′-TTCCTCATGGTCACATGGATGAGT-3′	This paper	N/A
RAGE primer: Forward 5′-GTGTCCTTCCCAACGGCTC-3′ Reverse 5′-ATTGCCTGGCACCGGAAAA-3′	This paper	N/A
TLR2 primer: Forward 5′-ATCCTCCAATCAGGCTTCTCT-3′ Reverse 5′-GGACAGGTCAAGGCTTTTTACA-3′	This paper	N/A
TLR4 primer: Forward 5′-AGTTGATCTACCAAGCCTTGAGT-3′ Reverse 5′-GCTGGTTGTCCCAAAATCACTTT-3′	This paper	N/A
Recombinant DNA		
pLKO-shHMGB1 #932	Sigma-Aldrich	TRCN0000018932
pLKO-shHMGB1 #934	Sigma-Aldrich	TRCN0000018934
pLKO-shHIF-1α #3808	Sigma-Aldrich	TRCN0000003808
pLKO-shHIF-1α #3809	Sigma-Aldrich	TRCN0000003809
pLKO-shHIF-2α #3805	Sigma-Aldrich	TRCN0000003805
pLKO-shHIF-2α #3806	Sigma-Aldrich	TRCN0000003806
pLKO-shCtr	Sigma-Aldrich	SHC002
Software and algorithms		
ImageJ	ImageJ Software	RRID:SCR_003070; https://imagej.nih.gov/ij/
GraphPad Prism 7	GraphPad Software	RRID:SCR_002798; https://www.graphpad.com/
GSEA software (vision 3.0)	Downloaded from the Broad Institute	http://www.broadinstitute.org/gsea

RESOURCE AVAILABILITY

Lead contact

Further information and requests for resources and reagents should be directed to and will be fulfilled by the lead contact, Xingjiang Yu (yuxingjiang@hust.edu.cn).

Materials availability

This study did not generate new unique reagents.

Data and code availability

- This paper analyzes existing, publicly available data. These accession numbers for the datasets are listed in the key resources table. All data reported in this paper will be shared by the lead contact upon request.
- This paper does not report original code.
- Any additional information required to reanalyze the data reported in this paper is available from the lead contact upon request.

EXPERIMENTAL MODEL AND SUBJECT DETAILS

Human studies

Glioma tissue was obtained from the department of neurosurgery in Tongji Hospital, Tongji Medical College, Huazhong University of Science and Technology, Wuhan, China. The classification of all glioma patients was based on the 2021 WHO classification of CNS tumors. Clinical information for GBM (WHO2021, IDH wt, Grade 4) patients were as follows: patient 2, male, 45 years old; patient 3, female, 43 years old; patient 4, male, 46 years old; patient 5, male, 54 years old; patient 6, female, 56 years old; patient 7, male, 61 years old; patient 8, female, 7 years old; patient 9, male, 51 years old; patient 10, male, 54 years old. patient 11, female, 53 years old. The tissue microarray included tumors from 11 patients with Grade 2 astrocytoma (IDH-mutant), 4 females, 7 males, ages 33–53 years old, median 44 years; 5 patients with Grade 3 astrocytoma (IDH-mutant), 3 females, 2 males, ages 43–59 years old, median 53 years; 24 patients with GBM (IDH wild-type), 6 females, 18 males, ages 26–65 years old, median 49 years. Normal brain tissue was from 3 females and 8 males. All participants signed informed consent. This study was permitted by the Ethics Committee of Tongji Hospital of Huazhong University of Science and Technology.

Mouse xenografts

The immunodeficient BALA/c Nude mice (4–5-week old) were purchased from Beijing Vital River Laboratory Animal Technology Co., Ltd. Five mice were allowed in one cage. Both male and female mice were used. The littermates of same sex were randomly assigned to different groups. For establishing GBM orthotopic mouse xenografts, 2×10^4 D456 GSCs with shNT or shHMGB1 were implanted into the right frontal lobes of mice (Man et al., 2018). For the survival analysis, mice were maintained until manifestation of neurological signs. For comparing tumor growth, different groups of mice implanted with GSCs were harvested on the same day as indicated after transplantation. Hematoxylin and eosin (HE) staining was performed to investigate tumor growth. Mice were euthanized when exhibiting declining neurologic status. After cardiac perfusion with PBS, brains were removed and fixed with 4% formaldehyde for 48 h, and then preserved in 30% sucrose at 4°C. All animal experiments were conducted according to protocols approved by the Institutional Animal Care and Committee of Tongji Medical College, Huazhong University of Science and Technology.

Cell lines

293T cells were used for virus production, which was cultured in DMEM supplemented with 10% fetal bovine serum, 100 units/mL penicillin, and 100 μg/mL streptomycin. Human glioma stem cell lines (T387 and D456) were kind gifts from Dr. Jeremy N Rich and Dr. Shideng Bao, which were isolated and characterized from GBM patients specimens as previously described (Man et al., 2018). GSC lines were maintained in Neurobasal-A medium containing B27 supplement, 1 mM L-Glutamine, 20 ng/mL EGF, 20 ng/mL FGF, 100 units/mL penicillin, and 100 μg/mL streptomycin. The expression of stem cell markers including Olig2, Sox2, as well as the absence of GFAP expression was assayed in GSCs. For obtaining the counterpart non-stem-like tumor cells (non-GSC), GSCs were differentiated in DMEM with 10% FBS for 12 days. Then, the expression of differentiation marker GFAP and stem markers including Sox2 and Olig2 was

detected. The GFAP positive cells without Sox2 and Olig2 expression were considered to be non-GSCs. Cells were grown under normal oxygen (21% O_2 and 5% CO_2) or hypoxic oxygen (1% O_2 and 5% CO_2) at 37°C. For inhibition of RAGE, 1μm or 5μm FPS-ZM1 was added to the medium when GSCs were cultured under hypoxia. 0μm FPS-ZM1 (DMSO treatment) served as control group. For stabilizing HIF-1α, 2mM dimethyloxalylglycine (DMOG), an analog of α-ketoglutarate known to inhibit prolylhydroxylase activity, was used to treat GSCs for 48h under normoxia (Li et al., 2015; Xu et al., 2022). 0mM DMOG (DMSO treatment) served as control group.

METHOD DETAILS

shRNA plasmids and lentiviral transfection

Lentiviral plasmids harboring short hairpin RNA (shRNA) targeting human shHMGB1 (#932, #934), human shHIF-1α (#3808, #3809) or human shHIF-2α (#3805, #3806) were purchased by Sigma-Aldrich. A non-targeting shRNA (shNT) control served as control. Lentivirus was produced in 293T cells. In brief, the plasmids were transfected with packaging plasmid psPAX2 and envelope plasmid VSV-G into 293T cells for 12 h. Then, the mediums were changed to Neurobasal-A medium, and cells were incubated for another 48 h. The mediums were collected and filtered with 0.45 μm filters. The lentivirus was stored at −80°C until used.

Immunohistochemistry (IHC) and immunofluorescent (IF) staining

The paraffin-embedded tissue microarray included non-neoplastic brain tissue and glioma tissue. IHC staining of tissue sections was performed with 2-step plus Poly-HRP Anti-Mouse/Rabbit IgG Detection System using DAB (3,30-Diaminobenzine) detection. In brief, after deparaffination, hydration and antigen retrieval, tissue sections were incubated with primary antibodies overnight at 4 °C. After being washed with PBS, the sections were then incubated with Polymer Helper for 20 minutes at 37°C followed by incubation with polyperoxidase-anti-mouse/rabbit IgG for 30 minutes at 37°C. Nuclei were stained with hematoxylin. Images were assessed with ImageJ software (Schneider et al., 2012).

For IF staing, GSCs were seeded on glass coverslips coated with Matrigel and cultured for 24h under hypoxic conditions. IF staining of frozen tissue sections was performed as previously described (Man et al., 2018). Briefly, cells or tissue specimens were fixed with 4% formaldehyde for 20 min at room temperature, followed by PBS washing. Samples were blocked with 5% normal donkey serum for 1 h after permeabilization with 0.5% Triton-X in PBS for 20 min at room temperature. And then samples were incubated with primary antibodies overnight at 4°C followed by incubation with appropriate fluorescent-labeled secondary antibodies for 1 h at room temperature. DAPI was used to stain nuclei. Images were obtained with a laser scanning confocal microscope (Olympus FV 1000). Images were assessed with ImageJ software.

RNA isolation and quantitative real-time PCR (qPCR)

Total RNA from GSCs was extracted using TRIZOL (Invitrogen) and subsequently converted to cDNA using a reverse transcription kit HiScript II Q RT SuperMix following the manufacturer's instruction. Quantitative PCR was performed with ChamQ SYBR qPCR Master Mix on StepOne Plus PCR instrument (Applied Biosystems) under the following cycle conditions: 95°C for 5 min, 40 cycles of 95°C for 10 s and 60°C for 30 s. All primers used for qPCR were listed in the key resources table. The relative mRNA expression to GAPDH was calculated and data were normalized to control group.

Western blot analysis

Cells were collected and lysed on ice using RIPA lysis buffer (150 mM sodium chloride, 50 mM pH8.0 Tris-HCL, 1% Nonidet P-40, 0.5% sodium deoxycholate, 0.1% SDS) containing protease and phosphatase inhibitors (MedChemExpress, USA). Protein lysates were separated on SDS-polyacrylamide gel and transferred to a polyvinylidene difluoride membrane. Then, the non-specific binding was blocked with 5% skim milk for 1 h at room temperature. The membranes were incubated with primary antibodies at 4°C overnight followed by washing with TBST three times. After being incubated with a peroxidase-conjugated secondary antibody for 1 h at room temperature, the binds were visualized with an ECL system. α-tubulin or GAPDH served as an internal control. All experiments were performed at least in triplicate. Bands were quantified using ImageJ software. Relative protein levels to internal controls (α-tubulin or GAPDH) were calculated and data were normalized to control group.

Cell viability assays

1×10^3 cells were plated into each well of 96-well plates, and were subjected to hypoxia for different days (0, 1, 3, 5 d). Cell titers were determined using the Cell Titer-Lumi^{TM} Plus Luminescent Cell Viability Assay Kit according to the manufacturer's protocol. Briefly, the reagent was added to the well to lyse the cells, followed by incubation for 10 min at room temperature. The luminescent signals were measured. The experiments were performed in triplicate. The data were normalized to day 0 and presented as mean ± SD.

5-ethynyl-20-deoxyuridine (EdU) incorporation assay

According to the manufacturer's protocol of Cell-Light EdU Apollo-567 *In Vitro* Imaging Kit, cells were incubated with EdU (1:5000) for 2 h, followed by PBS washing. After fixation with 4% formaldehyde for 30 min, the cells were incubated with glycine (2 mg/mL) and permeabilized with 0.5% Triton-X for 30 min. The cells were then mixed with Apollo reaction for 30 min. The nuclei were stained with DAPI. EdU incorporation was counted in 200 cells.

Tumorsphere formation assay and *in vitro* limiting dilution assay

GSCs were digested into single cells. 1000 cells were then seeded in 96-well plates per well. After 7 days under hypoxic conditions or 3 days under normoxic conditions, tumorsphere number of GSCs with shNT or shHMGB1was calculated. For detecting the effect of FPS-ZM1 on GSCs tumorsphere formation, GSCs were cultured under hypoxic conditions for 48h, tumorsphere number of GSCs was calculated.

For *in vitro* limiting dilution assay, GSCs were plated into 96-well plates with gradient cell concentrations of 1, 10, 20, 30, 40, and 50 cells per well, with 6 replicates for each concentration. After incubation for 7 days under hypoxic conditions, the number of tumorsphere in each well was determined. The efficiency of sphere formation was calculated using the Extreme Limiting Dilution Analysis (http://bioinf.wehi.edu.au/software/elda) (Hu and Smyth, 2009).

ELISA assay

Human blood samples were obtained at Tongji Hospital from 3 healthy donors and glioma patients prior to tumor resection including 8 astrocytoma (IDH mutant) Grade 2; 10 astrocytoma (IDH mutant) Grade 3; 15 GBM (IDH wt). GSCs were cultured under normoxia or hypoxia for 72h, the medium was collected and filtered for ELISA assay. The concentrations of HMGB1 in human serum or cell supernatants were quantified using Human HMGB1 ELISA kits according to the manufacturer's instructions. The absorbance was determined at 450 nm using a Thermomax microplate reader (Bio-Tek, USA). The experiment was repeated three times.

Bioinformatics analysis

Glioma database including RNA-seq, patient survival, and correlations of genes was downloaded from TCGA or CGGA Dababase (http://gliovis.bioinfo.cnio.es/). Gene Set Enrichment Analysis (GSEA) and Kyoto Encyclopedia of Genes and Genomes (KEGG) pathway enrichment analysis were applied to find the related functional pathway through which HMGB1 might affect GBM progression. The median level of the HMGB1 expression was used to classify the GBM patients with IDH wt into low- and high-expression groups based on clinical data from the CGGA dataset. 95 samples for each group were analyzed.

QUANTIFICATION AND STATISTICAL ANALYSIS

GraphPad Prism software 7.0 was used to perform the statistical analysis. All data were expressed as mean ± SD unless otherwise specified. All experiments *in vitro* were repeated at least three times. Statistical significance was assessed by using Mann-Whitney U test and two-tailed unpaired Student's t-test for the comparison of two groups or one-way ANOVA with Tukey's test for more than two groups. Kaplan-Meier survival curves were analyzed by using Log-rank test. The correlation of two gene expression from TCGA or CGGA database was analyzed by Pearson's correlation analysis. Differences were considered significant if $p < 0.05$.